

# On the relationship between $\delta\text{O}_2/\text{N}_2$ variability and ice sheet surface conditions in Antarctica

Romilly Harris Stuart<sup>1</sup>, Amaëlle Landais<sup>1</sup>, Laurent Arnaud<sup>2</sup>, Christo Buizert<sup>3</sup>, Emilie Capron<sup>2</sup>, Marie Dumont<sup>4</sup>, Quentin Libois<sup>5</sup>, Robert Mulvaney<sup>6</sup>, Anaïs Orsi<sup>1,7</sup>, Ghislain Picard<sup>2</sup>, Frédéric Prié<sup>1</sup>, Jeffrey Severinghaus<sup>8</sup>, Barbara Stenni<sup>9</sup>, and Patricia Martinerie<sup>2</sup>

<sup>1</sup>Laboratoire des Sciences du Climat et de l'Environnement, LSCE-IPSL, CEA-CNRS-UVSQ, Univ. Paris-Saclay, 91190 Gif-sur-Yvette, France

<sup>2</sup>Université Grenoble Alpes, CNRS, INRAE, IRD, Grenoble INP, IGE, 38000 Grenoble, France

<sup>3</sup>College of Earth, Ocean, and Atmospheric Sciences, Oregon State University, Corvallis, OR 97331, USA

<sup>4</sup>Univ. Grenoble Alpes, Université de Toulouse, Météo-France, CNRS, CNRM, Centre d'Etudes de la Neige, 38000 Grenoble, France

<sup>5</sup>CNRM, Université de Toulouse, Météo-France, CNRS, Toulouse, France

<sup>6</sup>British Antarctic Survey, Natural Environment Research Council, Madingley Road, Cambridge CB3 0ET, UK

<sup>7</sup>The University of British Columbia, Department of Earth, Ocean and Atmospheric Sciences, Vancouver, Canada

<sup>8</sup>Scripps Institution of Oceanography, University of California, San Diego, La Jolla, CA 92093, USA

<sup>9</sup>Ca' Foscari University of Venice, Department of Environmental Sciences, Informatics and Statistics, Venezia, 30172, Italy

**Correspondence:** Romilly Harris Stuart (romilly.harris-stuart@lsce.ipsl.fr)

**Abstract.** While the processes controlling pore closure are broadly understood, the physical mechanisms driving the associated elemental fractionation remains ambiguous. Previous studies have shown that the pore closure process leads to a depletion in small-sized molecules (e.g., H<sub>2</sub>, O<sub>2</sub>, Ar, Ne, He) in ice core bubbles relative to larger-sized molecules like N<sub>2</sub>. This size-dependent fractionation, identified using ice core  $\delta(\text{O}_2/\text{N}_2)$  records, exhibits a clear anti-correlation with local summer solstice insolation, making  $\delta(\text{O}_2/\text{N}_2)$  a valuable ice core dating tool. Mechanisms controlling this relationship are attributed to the physical properties of deep firn. In this study, we compile  $\delta(\text{O}_2/\text{N}_2)$  records from 15 polar ice cores and show a new additional link between  $\delta(\text{O}_2/\text{N}_2)$  and local surface temperature and/or accumulation rate. Using the Crocus snowpack model, we perform sensitivity tests to identify the response of near-surface snow properties to changes in insolation intensity, accumulation rate, and air temperature. These tests support a mechanism linked to firn grain size, such that the larger the grain size for a given density, the stronger the pore closure fractionation, and hence, the lower the  $\delta(\text{O}_2/\text{N}_2)$  values archived in the ice. Based on both snowpack model outputs and data compilation, our findings suggest that local accumulation rate and temperature should be considered when interpreting  $\delta(\text{O}_2/\text{N}_2)$  as a local insolation proxy.

## 1 Introduction

Ice cores store crucial information for our understanding of past climate variability and atmospheric composition. Interpreting ice core gas records first requires an understanding of the evolution of snow into ice via the firnification processes. Firn is the name given to the layer of consolidated snow which makes up the top 50-120 m of ice sheets. Atmospheric air moves through

porous networks within the firn until a critical depth (known as the lock-in depth) where vertical diffusion effectively stops, and pores gradually become sealed off from the atmosphere. The lock-in depth and the depth at which all pores are closed (close-off depth) are largely determined by local accumulation rate, temperature, and possibly the degree of density layering (Schwander et al., 1997; Martinerie et al., 1994; Mitchell et al., 2015). The region between the lock-in depth and close-off depth, where gases are progressively occluded into bubbles, is known as the lock-in zone (LIZ).

Gas records from ice cores provide a vital dating tool, especially at low accumulation sites where other methods are unsuitable. One such tool is orbital dating, which enables certain gas records to be tuned to insolation curves directly calculated from astronomical variables (Laskar, J. et al., 2004). For example, ice core  $\delta^{18}\text{O}_{\text{atm}}$  records ( $\delta^{18}\text{O}$  of atmospheric  $\text{O}_2$ ) are strongly correlated with precession (mid-June  $65^\circ\text{N}$  insolation) (Bender et al., 1994).  $\delta^{18}\text{O}_{\text{atm}}$  provides a direct atmospheric signal which may ultimately be used to align different ice core records (Extier et al., 2018). Two alternative proxies for orbital dating are 1) total air content, which is anti-correlated with integrated summer insolation, i.e., the annual sum of daily insolation above a certain threshold (Raynaud et al., 2007; Eicher et al., 2016), and 2)  $\delta(\text{O}_2/\text{N}_2)$ , which is anti-correlated with local summer solstice insolation intensity (e.g., Bender, 2002; Kawamura et al., 2007; Suwa and Bender, 2008b; Landais et al., 2012; Bouchet et al., 2023). Unlike  $\delta^{18}\text{O}_{\text{atm}}$ , TAC and  $\delta(\text{O}_2/\text{N}_2)$  reflect processes within the firn column making the records site specific. The term  $\delta(\text{O}_2/\text{N}_2)$  (hereafter, simply  $\delta\text{O}_2/\text{N}_2$ ) describes the relative difference between the ratio of  $\text{O}_2$  to  $\text{N}_2$  molecules trapped within the ice and that of the standard atmosphere and is expressed in the delta notation commonly used for stable isotope ratios.

The use of  $\delta\text{O}_2/\text{N}_2$  for dating was first proposed by Bender (2002) after observations of an anti-correlation between local summer solstice insolation (hereafter SSI) and  $\delta\text{O}_2/\text{N}_2$  from the Vostok ice core. A similar relationship was then observed at other sites such as Dome Fuji (Kawamura et al., 2007) and EPICA Dome C (Landais et al., 2012) in Antarctica, and GISP2 (Suwa and Bender, 2008b) in Greenland. Over orbital timescales,  $\delta\text{O}_2/\text{N}_2$  is in anti-phase with local SSI when drawn on the ice-age chronology, indicating that the firn properties controlling the  $\delta\text{O}_2/\text{N}_2$  fractionation are set near the surface. It is understood that increased temperature gradients under high SSI conditions enhances near surface snow metamorphism, thus increasing near-surface grain size which persists throughout the firnification process down to the close-off depth (Bender, 2002; Severinghaus and Battle, 2006; Suwa and Bender, 2008a; Fujita et al., 2009).

Parallel firn air studies of the open porosity revealed an enrichment in  $\text{O}_2$  and other small molecules (Ar, Ne and He) in the LIZ, providing further evidence of size-dependent fractionation during pore-closure (Battle et al., 1996; Huber et al., 2006; Severinghaus and Battle, 2006). While the physical mechanisms controlling the amount of fractionation are not fully understood, it is believed that smaller molecules ( $<3.6 \text{ \AA}$  diameter) escape during pore closure via molecular diffusion through the ice lattice (or permeation) driven by pressure gradients between recently closed pores and neighbouring open pores (Ikeda-Fukazawa et al., 2004; Huber et al., 2006; Severinghaus and Battle, 2006). This process is facilitated by the pore network's capacity to export the fugitive gases back to the atmosphere, which is required for the observed depletion of  $\text{O}_2$  in bubbles (Fujita et al., 2009).

In addition, Fujita et al. (2009) proposed that enhanced layering in the deep firn under high SSI conditions would also facilitate  $\delta\text{O}_2/\text{N}_2$  depletion. They argue that large-grained, relatively low-density 'summer' layers in the deep firn close-off deeper

and take longer to do so than neighbouring 'winter' layers (smaller-grained, relatively high density). As a result, 'summer' layers remain permeable for longer, allowing the O<sub>2</sub>-enriched air in the open porosity to be exported to the atmosphere, thereby reducing bulk ice  $\delta\text{O}_2/\text{N}_2$  under high SSI conditions (Fujita et al., 2009). While the proposed mechanisms are posited to explain the SSI imprint on  $\delta\text{O}_2/\text{N}_2$ , they are also influenced by local climate conditions such as temperature and accumulation rate. Indeed, there is a substantial amount of evidence linking local climate conditions with both firm physical properties (Casado et al., 2021; Inoue et al., 2023) and deep firm layering (Hörhold et al., 2011).

There is a growing body of evidence for a local climatic imprint on ice core  $\delta\text{O}_2/\text{N}_2$  records. Firstly, spectral analysis has revealed climate-related 100-kyr cyclicity at EPICA Dome C corresponding to glacial cycles (Bazin et al., 2016). However, this 100-kyr cyclicity is not apparent in the Dome Fuji  $\delta\text{O}_2/\text{N}_2$  record, which Kawamura et al. (2007) attribute to the idea that temperature and accumulation effects cancel each other out. Secondly, millennial-scale variability in  $\delta\text{O}_2/\text{N}_2$  records from the GISP2 core appeared in-phase with local temperature fluctuations driven by Dansgaard-Oeschger events (Suwa and Bender, 2008b). In contrast, Kobashi et al. (2015) evidenced an anti-phase effect of accumulation rate on  $\delta\text{Ar}/\text{N}_2$  records at GISP2 on decadal timescales over the last 6000 years. Like O<sub>2</sub>, Ar is a smaller molecule than N<sub>2</sub>, invoking the the same driving mechanisms for  $\delta\text{Ar}/\text{N}_2$  and  $\delta\text{O}_2/\text{N}_2$  variations, albeit the  $\delta\text{Ar}/\text{N}_2$  anomaly tends to be half as large as the  $\delta\text{O}_2/\text{N}_2$  anomaly (Bender et al., 1995; Buizert et al., 2023). Kobashi et al. (2015) proposed a direct effect of accumulation rate or temperature on the  $\delta\text{Ar}/\text{N}_2$  ( $\delta\text{O}_2/\text{N}_2$ ) variations through the firm depth. Higher accumulation rates (or lower temperatures) increase firm weight, leading to greater overloading pressures in microbubbles, which results in the preferential expulsion of Ar (O<sub>2</sub>) in the LIZ. Alternatively, Severinghaus and Battle (2006) proposed that higher accumulation rates result in more rapid the burial of bubbles, allowing less time for gases to escape during pore closure.

Using a combination of data compilation and snowpack modelling, we aim to develop our understanding of the formation of the  $\delta\text{O}_2/\text{N}_2$  records by first determining the role of local climate parameters, accumulation rate and temperature, on  $\delta\text{O}_2/\text{N}_2$  variability, and subsequently identifying potential mechanisms related to snow physical properties using snowpack sensitivity tests. We use a compilation of datasets from 15 ice cores from both Antarctica and Greenland to identify spatial and temporal patterns in  $\delta\text{O}_2/\text{N}_2$  depending on local surface conditions. The impacts of SSI and local climate on snow properties are then assessed using the SURFEX-ISBA-Crocus detailed snowpack model (Vionnet et al., 2012). We aim to constrain the influence of near-surface snow properties on  $\delta\text{O}_2/\text{N}_2$  variability, potentially contributing to a mechanistic explanation for elemental fractionation during pore closure.

## 2 Methods

### 2.1 Ice core sites

We compiled  $\delta\text{O}_2/\text{N}_2$  records from 18 ice cores from Antarctica and Greenland but use data from 15 of those sites for reasons explained in Section 2.2.3. Previously published data were measured on ice cores from: Dome Fuji (DF), EPICA Dome C (EDC), Greenland Ice Core Project 2 (GISP2), Law Dome DE08 and DSSW20k, North Greenland Ice core Project (NGRIP), Roosevelt Island Climate Evolution (RICE), Siple Dome (SD), South Pole (SP), Talos Dome (TALDICE), Vostok, and the

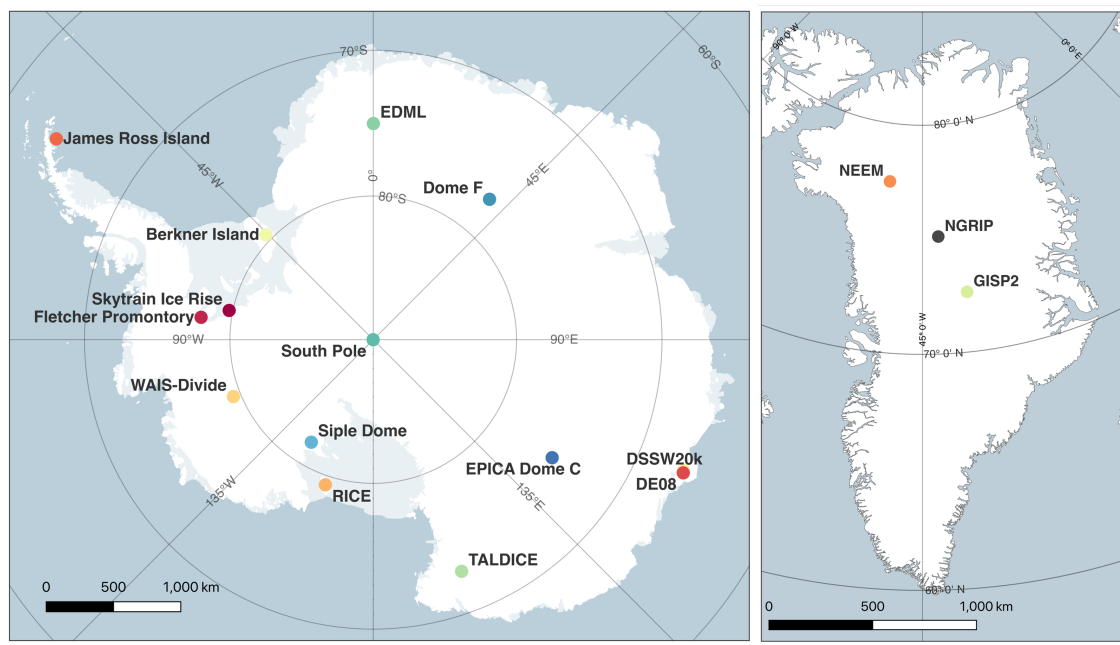


**Figure 1.** Locations of each ice core site initially included in our study (Matsuoka et al., 2018; Moon et al., 2023).

85 West Antarctic Ice Sheet Divide (WAIS) ice cores (references for all datasets are presented in Supplement Table S1). We also present unpublished data from Berkner Island (BI), EPICA Dronning Maud Land (EDML), Fletcher Promontory (FP), GISP2, James Ross Island (JRI), North Greenland Eemian Ice Drilling (NEEM), Skytrain Ice Rise (SIR) and Talos Dome (TALDICE) ice cores (overview of unpublished datasets in Supplement Table S2). Table 1 provides an overview of the site characteristics.

## 2.2 Analytical techniques for previously unpublished data

90 The previously unpublished  $\delta\text{O}_2/\text{N}_2$  datasets were measured at the Laboratoire des Sciences du Climat et de l'Environnement (LSCE), with the addition of new GISP2 data measured at Scripps Institution of Oceanography (Scripps). At both LSCE and Scripps, gases are extracted from the ice using a melt-refreeze technique based on the method described by Sowers et al. (1989) with modifications to the LSCE method as described by Landais et al. (2003), and to the Scripps method as outlined in Petrenko et al. (2006). In short, ice samples are placed into glass flasks at  $-20^\circ\text{C}$  while the atmospheric air is evacuated. Samples are  
 95 then left to slowly melt to release the trapped gases, before being refrozen. The extracted air samples are then passed through a  $\text{CO}_2$  and water vapour trap, before being trapped in the stainless-steel dip-tubes submerged in liquid helium. An alternative semi-automated extraction technique was also used at LSCE which removes the need for refreezing of the samples (Bazin et al., 2016; Bouchet et al., 2023).

**Table 1.** Overview of ice core site characteristics. The acronym BCTZ stands for brittle-clathrate transition zone, and COD stands for close-off depth.

Site	Latitude (°S)	Longitude (°E)	Elevation (m)	BCTZ <sup>a</sup> (m)	Accumulation rate <sup>b</sup> (cm w.eq yr <sup>-1</sup> )	Temperature <sup>c</sup> (°C)	COD <sup>d</sup> (m)
Berkner Island <sup>1</sup>	79.55	-45.68	890		16.2	-26	63
Dome Fuji <sup>2</sup>	77.32	39.7	3810	450–1200	2.6	-57.3	104
EPICA Dome C <sup>3</sup>	75.1	123.35	3233	600–1200	2.5	-54.5	100
EPICA Dronning Maud Land <sup>4</sup>	75	0.04	2892	700–1200	6.4	-44	83
Fletcher Promontory <sup>5</sup>	77.9	-82.61	873		38	-27	79
GISP2 <sup>6</sup>	-72.6	-38.5	3200	650–1400	22	-31.4	75
James Ross Island <sup>7</sup>	64.2	-57.69	1542		58	-14	67
DE08 <sup>8</sup>	66.72	113.2	1250		110	-19	88.5
DSSW20k <sup>9</sup>	66.77	112.81	1370		15	-20.7	53
NEEM <sup>10</sup>	-77.45	-51.6	2450	600–1200	20	-28.9	78.8
NGRIP <sup>11</sup>	-75.1	-42.32	3090	790–1200	17.5	-31.5	78
Roosevelt Island <sup>12</sup>	79.36	-161.71	550	763*	21	-23.5	52
Siple Dome <sup>13</sup>	81.65	-148.81	621	600-1000	12.4	-25.4	57.5
Skytrain Ice Rise <sup>14</sup>	79.74	-78.55	784		13.5	-26	58
South Pole <sup>15</sup>	89.99	-98.16	2835	619–1078	8	-49	125
Talos Dome <sup>16</sup>	72.82	159.07	2315	667–1002	8	-41	72
Vostok <sup>17</sup>	78.47	106.87	3488	250–900	2.2	-56	99.2
WAIS-Divide <sup>18</sup>	79.47	-112.09	1766	700–1300	20.2	-31.1	76.5

<sup>1</sup>Mulvaney et al., 2007<sup>a,b,c,d</sup>; <sup>2</sup>Oyabu et al., 2021<sup>a,d</sup>, Fujita et al., 1998<sup>b,c</sup>; <sup>3</sup>Parrenin et al., 2012, <sup>a</sup>EPICA community members, 2004<sup>b,c</sup>, Landais et al., 2006<sup>d</sup>; <sup>4</sup>Ueltzhöffer et al., 2010<sup>a</sup>, EPICA community members, 2006<sup>b,c,d</sup>; <sup>5</sup>Mulvaney et al., 2014<sup>a,b,c,d</sup>; <sup>6</sup>Gow et al., 1997<sup>a</sup>, Alley et al., 1993<sup>b</sup>, Alley and Koci, 1988<sup>c</sup>, Cuffey and Paterson, 2010<sup>d</sup>; <sup>7</sup>Mulvaney et al., 2014<sup>a,d</sup>, Capron et al., 2013<sup>b,c</sup>; <sup>8</sup>Etheridge et al., 1996<sup>a,b,c,d</sup>, Etheridge and Wookey, 1988<sup>b,c</sup>, Etheridge et al., 1996<sup>d</sup>; <sup>9</sup>Rubino et al., 2019<sup>a</sup>, Morgan et al., 1997<sup>b,c</sup>, Buizert and Severinghaus, 2016<sup>d</sup>; <sup>10</sup>Warming et al., 2013<sup>a</sup>, NEEM Community Members, 2013<sup>b,c</sup>, Buizert et al., 2012<sup>d</sup>; <sup>11</sup>NGRIP project members, 2004<sup>a,b,c</sup>, Martinerie et al., 2009<sup>d</sup>; <sup>12</sup>Lee et al., 2020<sup>a</sup>, Bertler et al., 2017<sup>b,c,d</sup>; <sup>13</sup>Gow and Meese, 2007<sup>a</sup>, Severinghaus et al., 2001<sup>b,c,d</sup>; <sup>14</sup>Mulvaney et al., 2021<sup>a,b,c</sup>, Hoffmann et al., 2022<sup>d</sup>; <sup>15</sup>Lazzara et al., 2012<sup>a</sup>, Severinghaus et al., 2001<sup>b,c,d</sup>; <sup>16</sup>Neff, 2014<sup>a</sup>, Stenni et al., 2002<sup>b,c</sup>; <sup>17</sup>Uchida et al., 1994<sup>a</sup>, Petit et al., 1999<sup>b,c</sup>, Cuffey and Paterson, 2010<sup>d</sup>; <sup>18</sup>Fitzpatrick et al., 2014<sup>a</sup>, Fegyveresi et al., 2011<sup>b,c</sup>, Battle et al., 2011<sup>d</sup>.

\*Reported bubble-clathrate transition depth corresponds to the maximum depth of RICE core (Lee et al., 2020).

### 2.2.1 New $\delta\text{O}_2/\text{N}_2$ measurements

100 Samples from the following sites were measured at LSCE, France on a 10-collector Thermo Delta V Plus Isotope Ratio Mass Spectrometer (IRMS), unless otherwise stated. This instrument allows for simultaneous measurements of elemental and

isotopic ratios, including  $\delta\text{O}_2/\text{N}_2$ ,  $\delta^{15}\text{N}-\text{N}_2$ , and  $\delta^{18}\text{O}-\text{O}_2$ . We note that  $\delta^{15}\text{N}-\text{N}_2$  data from the BI, EDML, JRI, and TALDICE samples were previously published by (Capron et al., 2013). In most cases, the values used in this study are the average of at least two replicate measurements and have an average analytical uncertainty of 0.5‰ for  $\delta\text{O}_2/\text{N}_2$ .

105 *Berkner Island*

Measurements were performed on bubbly ice from the BI ice core every 55 cm (every bag) between 631 m and 680 m, corresponding to 10,269–21,350 aBP (Capron et al., 2013). Replicate samples were prepared at LSCE using the melt-refreeze method between March 2010 and March 2011.

*EDML*

110 Nine samples were measured on bubbly ice from the EDML ice core over five depth levels between 328–473 m (327.8 m (4.51 ka BP), 354.2 m (4.95 ka BP), 381 m (5.43 ka BP), 467 m (7.04 ka BP), and 473 m (7.16 ka BP)) (Bazin et al., 2013). The samples were prepared using the melt-refreeze method at LSCE. Corresponding measurements of  $\delta^{15}\text{N}$  of  $\text{N}_2$  were previously published in (Capron et al., 2013).

*Fletcher Promontory*

115 In January 2015, 39 depth levels were measured from the FP ice core, retrieved in 2012. Measurements were performed approximately every 3 m starting at 289 m down to 388 m. There is currently no published age-scale for the FP ice core. All samples were prepared using the melt extraction method.

*James Ross Island*

120 Between February and March 2011, measurements were performed at 16 depth levels on the JRI ice core. The depth resolution varied between 2–50 m starting at 52 m until 363 m corresponding to 0.03–14.3 ka BP (Mulvaney et al., 2012). Samples were prepared using the melt extraction method.

*NEEM*

125 Clathrate ice from the NEEM ice core was measured between February and April 2011, a year after the core was retrieved. A total of 119 depth levels were sampled at varying resolutions over the following intervals: 55 cm intervals (every bag) between 1757–1773 m (38.127–39.735 kaB2k), 5.5 m intervals (every 10 bags) between 2205 and 2370 m (108.56–120.237 kaB2k), every 2 bags from 2375–2434 m (no published age-scale available below these depths), and 5.5 m intervals (every 10 bags) between 2436 and 2519 m (Gkinis et al., 2021; Rasmussen et al., 2013). Samples were prepared using the melt-refreeze method.

*Skytrain Ice Rise*

130 Measurements were performed on bubbly ice from the SIR ice core between March and April 2021. Samples were taken sporadically (1–15 m intervals) at 16 depth levels between 307 and 436 m depth (4.707–11.696 ka BP) (Mulvaney et al., 2023). Each sample was prepared at LSCE using the melt extraction method.

## TALDICE

135 Numerous measurements have been performed on bubbly and clathrate ice from TALDICE between 2008 and 2022 at LSCE. A total of 308 depth levels were measured at varying intervals starting at 155 m down to 1617 m. Published age-scales reach 1548 m, giving an age range of 1.55–343 ka for TALDICE samples (Buiron et al., 2011; Crotti et al., 2021). All samples were prepared using the melt extraction technique. Some measurements between 1356–1620 m depth have been published previously and are available in Crotti et al. (2021).

140 Samples from GISP2 were measured at Scripps on a 3kV Thermo Finnigan Delta V plus dual inlet IRMS. All measurements were measured in replicate.

## GISP2

145 Two datasets were measured on GISP2 ice. The first were measured in 2009 at 266 depth intervals from 318.67–1201.22 m. The second set of measurements were performed on samples from 643 depths between 1740 and 2400 m (13–50 ka BP) over several measurement campaigns between 2017–2020. The  $\delta^{15}\text{N}$  of  $\text{N}_2$  data from these samples were previously reported (Martin et al., 2023). In both cases, gases were extracted using the melt-refreeze technique and all measurements were referenced to La Jolla pier air.

### 2.2.2 Corrections

Chemical slope and pressure imbalance corrections are applied to the measurements during data processing (Landais et al., 2003). In addition, all data are corrected for gravitational fractionation in the firn using  $\delta^{15}\text{N}$  of  $\text{N}_2$  from the same samples.

$$150 \delta\text{O}_2/\text{N}_2 \text{ grav. corr.} = \delta\text{O}_2/\text{N}_2 - 4 \cdot \delta^{15}\text{N} \quad (1)$$

155 Gas loss effects during ice core storage are well documented to modify  $\delta\text{O}_2/\text{N}_2$ , causing significant depletion in  $\text{O}_2$  in clathrate ice stored above  $-50^\circ\text{C}$  (Ikeda-Fukazawa et al., 2005; Kawamura et al., 2007; Landais et al., 2012). Ikeda-Fukazawa et al. (2005) proposed a correction for storage gas loss effects as a function of temperature and time. However, given the incomplete storage history for all ice cores we do not attempt to correct for storage gas loss, but rather define rejection criteria outlined in Section 2.2.3.

### 2.2.3 Data rejection criteria

160 Ice core storage histories need to be considered before interpreting the data to account for post-coring gas loss effects which disturb the signal (Section 2.2.2). Successive  $\delta\text{O}_2/\text{N}_2$  measurements from TALDICE and GISP2 clathrate ice samples stored above  $-50^\circ\text{C}$  show strong depletion of  $\text{O}_2$  through time (Supplement S1), which is consistent with observations from EDC (Bouchet et al., 2023). We systematically reject measurements from clathrate ice stored at  $-20^\circ\text{C}$  for over 3 years, or at  $-36^\circ\text{C}$  for more than 4 years. Bubbly ice stored at these same temperatures appear to be mostly unaffected by gas loss (Supplement S1.2), with the exception of Vostok (Bender, 2002).

Several measurements were performed on ice within the bubble-clathrate transition zone (BCTZ), where high hydrostatic pressure in bubbles cause entrapped gases to form clathrate hydrates (Schaefer et al., 2011). At these depths, elemental fractionation occurs due to some gas species being preferentially incorporated into the clathrate structures (Ikeda-Fukazawa et al., 2001), thus making the interpretation of gas measurements unreliable (Bender, 2002). Measurements from the BCTZ may either have increased mean  $\delta\text{O}_2/\text{N}_2$  (usually in excess of 0‰) or strong data scattering, expressed as a high standard deviation (Oyabu et al., 2021). To avoid adding biases to our analysis, measurements from BCTZ are removed (Supplement S1.1). Additional scattering in elemental ratios, characterised by a standard deviation of 6.2‰ compared to 1.8‰ in pure bubble and clathrate ice, is observed below the BCTZ in the WAIS record between 1300–1500 m (Shackleton, 2019). Similar effects have been documented in the EDC and TALDICE ice cores (Lüthi et al., 2010), and the Dome Fuji ice core (Oyabu et al., 2021). Data influenced by this scattering effect were also removed from our analysis, followed by the removal of outliers ( $2\sigma$ ) from the cleaned datasets.

We note that these criteria result in the removal of all data from NGRIP, as well as sections of data from other sites (Supplement S1 for overview). We also exclude FP and SIR due to limited availability of accumulation rate and temperature records over the depth/age ranges covered by the  $\delta\text{O}_2/\text{N}_2$  data. The remaining 15 datasets are presented in Table 3 and were used to analyse the drivers of  $\delta\text{O}_2/\text{N}_2$  variability.

### 2.3 Modelling near-surface snow properties

The second component of our study addresses the modelled response of snow physical properties to perturbations in SSI, accumulation rate, and temperature with the aim of identifying which properties may be influencing elemental fractionation during pore closure. We use the SURFEX-ISBA-Crocus detailed snowpack model (Crocus hereafter) to simulate snowpack evolution (Vionnet et al., 2012). Crocus simulates changes in snow physical properties induced by surface metamorphism and the evolution of these properties with depth. The model is forced by ERA5 reanalysis data (Hersbach et al., 2020), and the snowpack is initialised with measurements of snow density, effective optical radius of snow grains and snow temperature. Optical radius is defined as the radius which snow grains would have for their surface area-to-volume ratio if they were spherical (Domine et al., 2006). Optical radius is thus directly linked to specific surface area (SSA), defined as the surface area of snow at the ice-air interface per unit mass (units  $\text{m}^2\text{kg}^{-1}$ ) (Legagneux et al., 2002), via the following equation:

$$\text{SSA} = \frac{3}{r_{\text{opt}} \cdot \rho_{\text{ice}}} \quad (2)$$

Where  $r_{\text{opt}}$  is the optical radius and  $\rho_{\text{ice}}$  is the density of ice (Gallet et al., 2014). We use this model to assess changes in snow physical properties near the surface which are invoked to explain  $\delta\text{O}_2/\text{N}_2$  variability. Dome C is used as the test site given the abundance of snowpack observations as well as high resolution  $\delta\text{O}_2/\text{N}_2$  data.

#### 2.3.1 Crocus model description

Crocus is a 1-dimensional model which simulates the evolution of snow properties with time and depth on a layer-by-layer basis, i.e., in a Lagrangian framework (Vionnet et al., 2012). A detailed description of the model can be found in Vionnet et al.



195 (2012). Briefly, the initial number of layers is defined by the user, with the thickness of each layer allowed to change along the simulation (layer thickness ranging from 2 mm at the surface to metres thick). The maximum number of layers available in the model was increased from 50 (Libois et al., 2014) to 80 (this study) to maximise the resolution with depth owing to the higher number of thin layers forming at Dome C than at Alpine sites. Once the simulated snowpack consists of 80 layers, the aggregation scheme merges internal neighbouring layers with similar properties allowing a new surface layer to form. The  
200 key physical processes incorporated into Crocus for dry snow conditions are accumulation of snowfall, snow metamorphism, compaction of snow by the wind, compaction due to the weight of the overlaying layers, absorption of solar radiation, heat diffusion, and surface energy budget.

For our study, two fundamental user-defined model components are the snow metamorphism and radiative transfer schemes. We use the semi-empirical model from Flanner and Zender (2006) (F06) for the metamorphism scheme which describes  
205 the evolution of optical radius with time. F06 was found to be the most appropriate formulation for Dome C conditions (Carmagnola et al., 2014; Libois et al., 2014). To successfully reproduce the snow temperature profile – vital for realistically simulating snow metamorphism – the Two-streAm Radiative TransfEr in Snow model (TARTES) is used to account for vertical distribution of absorbed solar radiation in the snowpack (Libois et al., 2013). TARTES also considers the effect of impurities on snow temperature via albedo. For Dome C, we include black carbon content which is set to  $3 \text{ ng g}^{-1}$  (Warren et al., 2006;  
210 Libois et al., 2015). Here we assess the simulated snow density, snow temperature, and snow SSA from Crocus model outputs.

### 2.3.2 Dome C specific Crocus configuration

Crocus was initially developed for alpine or sub-polar regions with seasonal snowpacks. Libois et al. (2014) modified multiple components of the Crocus model to improve its suitability to high latitude sites with low accumulation rates - specifically for Dome C. The modifications are extensively described in Libois et al. (2014) and were implemented into the current version of  
215 Crocus for this study. The changes are as follows:

1. *Fresh snow properties*: The parameterisation of fresh snow density is based on temperature and wind-speed which results in an unrealistically low density for Dome C ( $50 \text{ kg m}^{-3}$ ). Fresh snow density is fixed to a minimum of  $170 \text{ kg m}^{-3}$ , the lowest fifth percentile from Dome C observations (Libois et al., 2014). Similarly, fresh snow SSA is set to  $100 \text{ m}^2 \text{ kg}^{-1}$  instead of  $65 \text{ m}^2 \text{ kg}^{-1}$  used in the standard version of the model (Grenfell et al., 1994; Libois et al., 2014).
- 220 2. *Wind-induced compaction*: At low-accumulation sites, snow remains at the surface for prolonged periods of time. The long exposure time to surface winds facilitates compaction, and hence, increases density. The maximum surface snow density is increased from  $350 \text{ kg m}^{-3}$  to  $450 \text{ kg m}^{-3}$  to account for this effect (Albert et al., 2004; Libois et al., 2014).
- 225 3. *Aggregation scheme*: The formation of a new snow layer requires a minimum amount of snowfall. Due to the low accumulation rate at Dome C, the amount of snowfall needed to form a new layer was decreased from  $0.03 \text{ mm h}^{-1}$  to  $0.003 \text{ mm h}^{-1}$ . In the instance when the snowpack has the maximum number of layers (80) at the time a new snow layer is formed, layers with similar properties will be aggregated, resulting in a smoothed signal. The aggregation scheme was

disabled for the top 6 layers to resolve realistic near-surface snow temperature profiles, required to accurately simulate snow metamorphism.

### 2.3.3 Model initialisation

230 The snowpack was initialised with density and optical radius profiles measured in January 2010 at Dome C down to 20 m (Champollion et al., 2019), and snow temperature data from a probe installed at Dome C in 2012 with 5 cm resolution near the surface, coarsening with depth down to 12 m. ERA5 reanalysis data for Dome C was used to force the model at 3-hourly resolution over the period between 1 January 2000 and 1 December 2020 (Hersbach et al., 2020). The model requires atmospheric forcings for air temperature, accumulation rate, wind speed and direction, incoming shortwave and longwave radiation, 235 and specific humidity. ERA5 gives a mean annual snowfall rate between 2000 and 2020 of  $2.3 \text{ cm w.eq. yr}^{-1}$ , and as such, the snowfall rate was multiplied by 1.2 to match the observed mean annual accumulation rate of around  $2.8 \text{ cm w.eq. yr}^{-1}$  (Frez-zotti et al., 2004; Libois et al., 2014). To ensure that at least the top 1 m consists of accumulated snow, a 100-year spin up was used by running the forcing file ten times between 2000 and 2010, followed by the period from 2000 to 2020. The outputs from 2010 to 2020 were then used for analysis.

### 240 2.3.4 Sensitivity tests

The sensitivity of snowpack properties to perturbations in surface forcings are tested by modifying one of three forcing parameters: incoming shortwave radiation, accumulation rate, or 2 m air temperature. The magnitude of the perturbation to each parameter correspond to minimum and maximum values reconstructed over the last 800 ka. We use shortwave radiation as a proxy of insolation and scale the values in proportion to the SSI values. A total of seven simulations are used to perform 245 sensitivity analysis and are outlined in Table 2. The model configuration and initial snow profile were kept constant for each simulation; only the tested parameter in the atmospheric forcing file was modified as follows:

*Summer solstice insolation (SSI)*: Over the last 1000 years, the average SSI at  $75.1^\circ\text{S}$  was  $544 \text{ W m}^{-2}$  (Laskar, J. et al., 2004), compared to a minimum of  $462 \text{ W m}^{-2}$  and a maximum of  $601 \text{ W m}^{-2}$  over the past 800 ka. To translate to forcing perturbations, the incoming shortwave radiation (SWR) is scaled by 85% and 111%, respectively to reach the target 250 values ( $462 \text{ W m}^{-2}$  and  $601 \text{ W m}^{-2}$ ). No additional modifications are applied to annual distribution of SWR.

*Annual mean accumulation rate (A)*: Present-day accumulation rate at Dome C is set to  $2.8 \text{ cm w.eq. yr}^{-1}$  following Libois et al. (2014). Hereafter, accumulation rates expressed as water equivalent centimetres per year in the form  $\text{cm yr}^{-1}$ . ERA5 snowfall was scaled by 36% to reach the target accumulation rate of  $1.0 \text{ cm yr}^{-1}$ , representing the 800 ka minimum, and 146% to produce an accumulation rate of  $4.1 \text{ cm yr}^{-1}$  which corresponds to the 800 ka maximum (Bazin et al., 2013).

255 *Annual mean air temperature (T)*: Snowpack sensitivity to air temperature is tested by decreasing the 2 m air temperature by  $10^\circ\text{C}$  for glacial conditions (Jouzel et al., 2007), and applying a  $4^\circ\text{C}$  increase to represent 800 ka maximum temperatures. We note, however, that borehole temperature measurements and delta-age are more consistent with a  $5^\circ\text{C}$  cooling

(Buizert et al., 2021). Furthermore, these temperature modifications do not include changes in seasonal temperature variability but suffices for the purpose of identifying bulk changes in the snow properties. The average seasonal cycle is kept constant with an average amplitude of 35°C.

**Table 2.** Overview of modifications made to forcing test parameter in Crocus snowpack sensitivity test scenarios.

Simulation	Reference	SSI min	SSI max	A min	A max	T min	T max
Incoming SWR (Scaled)	100%	<b>85%</b>	<b>111%</b>	100%	100%	100%	100%
Accumulation rate (cm yr <sup>-1</sup> )	2.8	2.8	2.8	<b>1.0</b>	<b>4.1</b>	2.8	2.8
Air temperature (°C)	-55	-55	-55	-55	-55	<b>-65</b>	<b>-51</b>

It is important to highlight that, at polar sites, accumulation rate is dependent on temperature, and temperature is influenced by insolation, such that these parameters are not independent. However, we use the model to constrain the influences of each forcing parameter in an independent manner to understand the mechanisms, even if, in reality, these parameters are inter-dependent.

## 265 3 Results

### 3.1 Influence of SSI and local climate on $\delta\text{O}_2/\text{N}_2$ variability in ice cores

Figure 2 shows  $\delta\text{O}_2/\text{N}_2$  versus SSI for EDC, Dome F and South Pole. These three sites are used owing to their temporal range and high-resolution  $\delta\text{O}_2/\text{N}_2$  measurements, largely uninfluenced by gas loss. The regression slopes vary between  $-0.09 \pm 0.006\text{‰ W}^{-1}\text{m}^2$  for South Pole to  $-0.06 \pm 0.005\text{‰ W}^{-1}\text{m}^2$  for EDC. The regression for Dome F falls within 2 standard deviations ( $2\sigma$ ) of the regression for EDC, but the regression for South Pole falls outside this uncertainty.  $\delta\text{O}_2/\text{N}_2$  values from South Pole are higher than for EDC and Dome F for the same SSI, suggesting additional factors are influencing the records, such as accumulation rate, which at South Pole is around three times that of both EDC and Dome F. In the following sections, we provide evidence for the influences of accumulation rate and air temperature on  $\delta\text{O}_2/\text{N}_2$ , in addition to SSI, using both spatial (inter-site) and temporal (EDC ice core) variability of  $\delta\text{O}_2/\text{N}_2$ .

#### 275 3.1.1 Inter-site comparison of mean $\delta\text{O}_2/\text{N}_2$

In addition to the  $\delta\text{O}_2/\text{N}_2$  datasets, we compile SSI, accumulation rate, and temperature reconstructions for each site over the age/depth ranges which overlap in all records (Table 3). Drivers of mean  $\delta\text{O}_2/\text{N}_2$  are then explored using regression analysis, as presented in Fig. 3. Due to limited data availability from the BI ice core, we take an average temperature and accumulation rate using present day and last glacial maximum values presented in Capron et al. (2013). This is justified given the  $\delta\text{O}_2/\text{N}_2$  data spans approximately the last glacial maximum to the start of the Holocene (Massam, 2018). Present-day values are used for accumulation rate and temperature at DE08 and DSSW20k due to the relatively young ages corresponding to the  $\delta\text{O}_2/\text{N}_2$  data ( $\sim 90$  a BP).

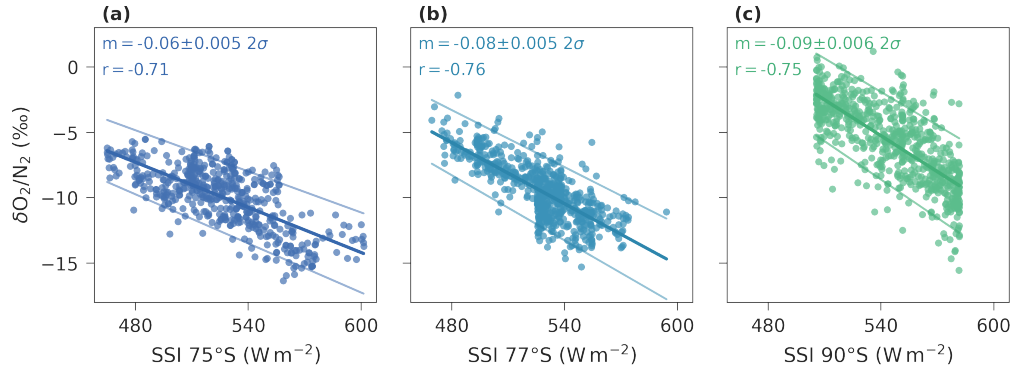


**Figure 2.** Scatter plots showing the relationship between SSI and  $\delta\text{O}_2/\text{N}_2$  at three Antarctic sites. Significant negative correlations (over 99% confidence) are observed using relatively high resolution data from (a) EDC (Bouchet et al., 2023), (b) Dome F (Kawamura et al., 2007; Oyabu et al., 2021), and (c) South Pole (Severinghaus, 2019). The slope ( $m$ , units  $\text{‰ W}^{-1}\text{m}^2$ ) and  $r$  values are presented for each site.

Figure 3 indicates significant correlations between mean  $\delta\text{O}_2/\text{N}_2$  and all surface variables (SSI, accumulation rate, and temperature). Mean SSI appears to have the weakest influence on mean  $\delta\text{O}_2/\text{N}_2$  (Fig. 3a;  $r=-0.46$ ,  $p<0.1$ ), but a slope of  $-0.09 \pm 0.05 \text{‰ W}^{-1}\text{m}^2$  is statistically indistinguishable from the temporal slope ( $-0.07 \text{‰ W}^{-1}\text{m}^2$ ; Fig. 2). The weaker spatial correlation may be linked to the small range in SSI between sites compared to the temporal range of SSI at an individual site. Figure 3b and 3c show a strong, significant correlations between mean  $\delta\text{O}_2/\text{N}_2$  and both the natural log of accumulation rate ( $r=0.86$ ,  $p<0.0001$ ) and temperature ( $r=0.79$ ,  $p<0.005$ ). The log-linear model in Fig. 3b indicates that a doubling of

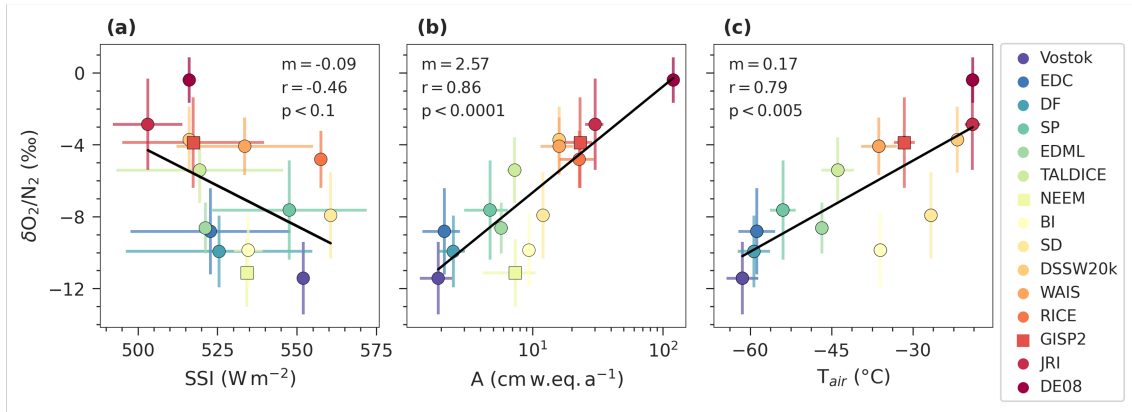


**Figure 3.** Scatterplots showing the dependence of  $\delta\text{O}_2/\text{N}_2$  on a) SSI, b) accumulation rate ( $A$ ), and c) air temperature ( $T_{air}$ ). Each point represents the mean values of each site over the depth interval in Table 3, with error bars showing the standard deviation ( $1\sigma$ ). Sites from Greenland are identified by square markers. Linear regressions are shown in black, along with the associated slope ( $m$ , units  $\text{‰ W}^{-1}\text{m}^2$ ), correlation coefficient ( $r$ ), and  $p$ -value ( $p$ ).

**Table 3.** Overview of data used in Fig. 3. Mean values are presented for  $\delta\text{O}_2/\text{N}_2$ , accumulation rate (in water equivalent), temperature, and SSI at the current site latitude (Laskar, J. et al., 2004). Where age scales are available, the SSI represents the mean values at the present day site latitude. For sites without age scales, the average SSI over last 1000 years is used.

Site	Depth range (m)	Age range (ka BP)	$\delta\text{O}_2/\text{N}_2^a$ (‰)	Accum. <sup>b</sup> ( $\text{cm yr}^{-1}$ )	Temp. <sup>c</sup> (°C)	SSI ( $\text{W m}^{-2}$ )
BI <sup>1</sup>	631–694	~10–20	$-9.9 \pm 2.0$	2.5	-45	535
DF <sup>2</sup>	113–450, 1504–2500	2.9–15.8, 102.0–207.8	$-9.9 \pm 2.0$	2.4	-59.3	526
EDC <sup>3</sup>	1421–3189	105.9–805.1	$-8.8 \pm 2.1$	2.1	-58.8	523
EDML <sup>4</sup>	595–693	9.8–12.0	$-8.6 \pm 1.4$	5.8	-46.8	521
GISP2 <sup>5</sup>	73–650, 1400–1674	0.17–2.9, 8.3–11.6	$-3.9 \pm 2.5$	23.1	-31.6	517
JRI <sup>6</sup>	52–359	-0.002–12.8	$-2.9 \pm 2.5$	30.2	-19.0	503
LD (DE08) <sup>7</sup>	175–218	0.008–0.011	$-0.4 \pm 1.3$	110.3	-19.0	516
LD (DSSW20k) <sup>8</sup>	61–63		$-3.7 \pm 1.8$	14.7	-21.8	516
NEEM <sup>9</sup>	1757–1773	38.1–39.7	$-11.1 \pm 1.9$	7.4		534
RICE <sup>10</sup>	70–342	0.2–2.6	$-4.8 \pm 1.6$	20.9		557
SD <sup>11</sup>	69–395	0.4–5.2	$-7.9 \pm 2.4$	12.0	-26.7	561
SP <sup>12</sup>	125–619, 1078–1727	1.1–19.7, -52.8	$-7.6 \pm 2.8$	4.7	-54.0	548
TALDICE <sup>13</sup>	155–667, 1002–1069	1.5–11.5, 34.7–124.6	$-5.4 \pm 1.8$	7.3	-43.8	519
Vostok <sup>14</sup>	2503–3272	201.8–408.4	$-11.4 \pm 2.0$	1.9	-61.4	552
WAIS <sup>15</sup>	80–700, 1500–3397	0.2–2.9, 7.4–66.2	$-4.1 \pm 1.6$	16.0	-36.5	533

<sup>1</sup>This study<sup>a</sup>, Capron et al., 2013<sup>b,c</sup>

<sup>2</sup>Kawamura et al., 2007<sup>a</sup>, Oyabu et al., 2021<sup>a</sup>, Kawamura et al., 2017<sup>b</sup>, Uemura et al., 2018<sup>c</sup>

<sup>3</sup>Bouchet et al., 2023<sup>a</sup>, Bazin et al., 2013<sup>b</sup>, Jouzel et al., 2007<sup>c</sup>

<sup>4</sup>This study<sup>a</sup>, Bazin et al., 2013<sup>b</sup>, Stenni et al., 2010<sup>c</sup>

<sup>5</sup>This study<sup>a</sup>, Bender et al., 1994<sup>a</sup>, Smith, 1998<sup>a</sup>, Suwa and Bender, 2008b<sup>a</sup>, Cuffey and Clow, 1999<sup>b</sup>, Clow, 1999<sup>c</sup>

<sup>6</sup>This study<sup>a</sup>, Mulvaney et al., 2012<sup>b,c</sup>, Capron et al., 2013<sup>b,c</sup>

<sup>7</sup>Buizert et al., 2020<sup>a</sup>, Etheridge and Wookey, 1988<sup>b,c</sup>

<sup>8</sup>Buizert et al., 2020<sup>a</sup>, Morgan et al., 1997<sup>b,c</sup>

<sup>9</sup>This study<sup>a</sup>, Rasmussen et al., 2013<sup>b</sup>

<sup>10</sup>Lee et al., 2020<sup>a</sup>, Winstrup et al., 2019<sup>b</sup>

<sup>11</sup>Severinghaus, 2009<sup>a</sup>, Buizert, 2021<sup>b,c</sup>;

<sup>12</sup>Severinghaus, 2019<sup>a</sup>, Kahle et al., 2020<sup>b,c</sup>

<sup>13</sup>This study<sup>a</sup>, Crotti et al., 2021<sup>a</sup>, Bazin et al., 2013<sup>b,c</sup>

<sup>14</sup>Bender, 2002<sup>a</sup>, Suwa and Bender, 2008a<sup>a</sup>, Bouchet et al., 2023<sup>b</sup>, Petit et al., 1999<sup>c</sup>

<sup>15</sup>Severinghaus, 2015<sup>a</sup>, Fudge et al., 2017<sup>b</sup>, White et al., 2019<sup>c</sup>.

accumulation rate would result in a 1.4‰ increase in  $\delta\text{O}_2/\text{N}_2$  ( $\delta\text{O}_2/\text{N}_2 = 2.6 \cdot \log(A) - 12.6$ ). However, it is important to  
290 note that temperature and the logarithm of accumulation rate are strongly correlated in Antarctica, such that the correlations  
seen in panels (b) and (c) of Fig. 3 are dependent on one another.

Deviations from the regression lines in Fig. 3 may have multiple origins, such as discrepancies in site latitude resulting from  
the ice flow speeds at different sites, or simply uncertainties in the records. For BI and SD, we consider that the relatively low  
 $\delta\text{O}_2/\text{N}_2$  values may be the result of storage gas loss effects (Section 2.2.3 and Supplement S1) given that the measurements  
295 were carried out  $\sim 7$  and  $\sim 8$  years after coring for BI and SD, respectively. While clathrates are reportedly absent from BI  
(Mulvaney et al., 2007; Neff, 2014), and SD data was removed below 600 m, the depth at which clathrate-like features first  
appear (Gow and Meese, 2007), the low values may link to gas loss during storage within increasingly brittle ice at depth in  
the core. Indeed, brittle ice is reported from 450 m at BI and 400 m at SD (Neff, 2014).

### 3.1.2 Temporal variability of $\delta\text{O}_2/\text{N}_2$ at Dome C

300 High resolution data is required to investigate the temporal variability in  $\delta\text{O}_2/\text{N}_2$  as a function of accumulation rate and  
temperature. The  $\delta$ -deuterium ( $\delta\text{D}$ ) record from water isotope measurements is used as a qualitative proxy for accumulation  
rate and temperature, whereby higher  $\delta\text{D}$  values are generally associated with increased accumulation rate and temperature in  
ice cores from the East Antarctic plateau (Jouzel et al., 2007; Parrenin et al., 2007). The following analysis uses the longest  
period of relatively high-resolution  $\delta\text{O}_2/\text{N}_2$  measurements from the EDC ice core between 190–259 ka BP (1980–2350 m) on  
305 the AICC2023 ice-age chronology (Bouchet et al., 2023).

Two approaches are used to extract the non-SSI signals in the  $\delta\text{O}_2/\text{N}_2$  records. First, we interpolate SSI onto the  $\delta\text{O}_2/\text{N}_2$  ages  
and take the deviations from the  $\delta\text{O}_2/\text{N}_2$ -SSI linear regression to isolate the  $\delta\text{O}_2/\text{N}_2$  variability not explained by SSI (hereafter,  
 $\delta\text{O}_2/\text{N}_2$ -SSI residual). The second approach directly investigates the millennial-scale variability by applying a low pass filter  
to the  $\delta\text{O}_2/\text{N}_2$  and  $\delta\text{D}$  records (interpolated onto a 100-year time step), using a 10-kyr cut-off to isolate the low-frequency  
310 signals associated with SSI. The filtered curves are then subtracted from the original curves to remove the orbital (SSI) signal,  
and a 5-point moving average is applied to the residuals to reduce noise but retain millennial-scale variability in the records.

Figure 4 primarily shows the dominant SSI cyclicity in the  $\delta\text{O}_2/\text{N}_2$  record, as has been documented previously (e.g., Landais  
et al., 2012). Superimposed onto this signal are millennial-scale peaks in  $\delta\text{O}_2/\text{N}_2$  which appear to coincide with peaks in  $\delta\text{D}$ ,  
highlighted by grey bars. This high frequency variability is more clearly identified from the filtered curves in Fig. 4d and  
315 4e. The coherence between millennial-scale peaks in  $\delta\text{O}_2/\text{N}_2$  and  $\delta\text{D}$  suggests a positive correlation with accumulation rate  
and temperature, which shares analogy with the positive spatial correlation between  $\delta\text{O}_2/\text{N}_2$  and both accumulation rate and  
temperature (Fig. 3). We note a remnant 20-kyr variability in the  $\delta\text{O}_2/\text{N}_2$ -SSI residual, in phase with  $\delta\text{D}$ , which is present  
when using either the AICC2012 chronology (Bazin et al., 2013) or the AICC2023 chronology (Bouchet et al., 2023). Given  
that the new AICC2023 age scale (used here) has been orbitally tuned using this data (Bouchet et al., 2023), this signal is not  
320 expected to be the result of phase difference between the EDC chronology and SSI.

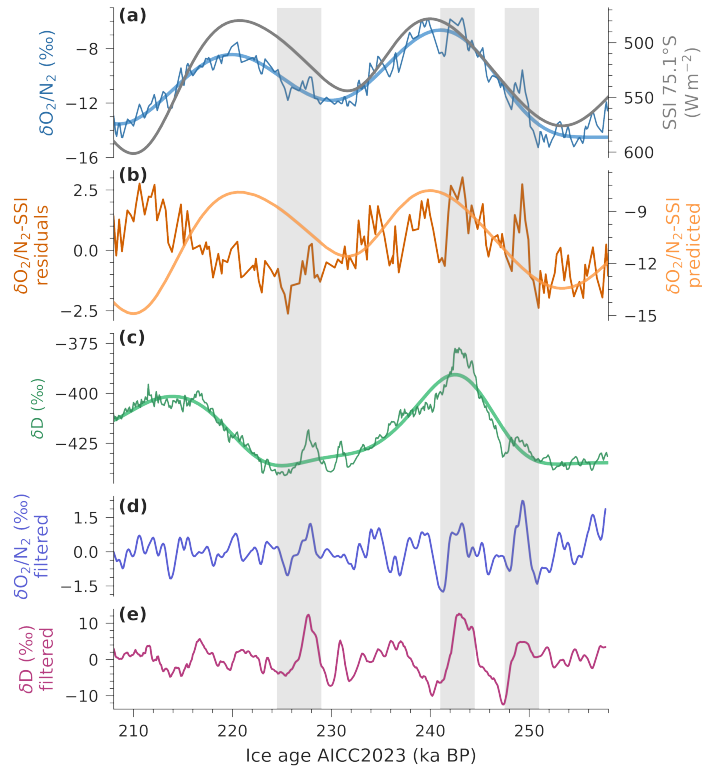


**Figure 4.** Evolution of  $\delta\text{O}_2/\text{N}_2$ , SSI, and  $\delta\text{D}$  on the AICC2023 ice age timescale from EDC (Bouchet et al., 2023). Panel (a) presents the 100-year interpolated  $\delta\text{O}_2/\text{N}_2$  overlain with the low pass filtered curve (blue). The right y-axis in panel (a) shows SSI at  $75.1^\circ\text{S}$  (grey). The predicted  $\delta\text{O}_2/\text{N}_2$  as a function of SSI ( $\delta\text{O}_2/\text{N}_2$ -SSI predicted) is shown on the right axis of panel (b), and the residuals of the observed  $\delta\text{O}_2/\text{N}_2$  and predicted are on the left axis. Panel (c) shows the 100-year interpolated  $\delta\text{D}$  overlain with the low pass filtered curve (green). The bottom two panels present the residuals of the low pass filtered curves for  $\delta\text{O}_2/\text{N}_2$  (d) and  $\delta\text{D}$  (e). Grey bars highlight the pronounced millennial-scale variability.

## 3.2 Crocus model results

### 3.2.1 Crocus model evaluation for Dome C

The Crocus model outputs are first evaluated by comparing the reference simulation (Ref in Table 2) to observational data from Dome C. Simulated density and SSA profiles are compared to data from Libois et al. (2014), measured daily between 23  
 325 November 2012 and 16 January 2013 at two sites within 600 m of Concordia station, Dome C. Density was measured at 2.5 cm resolution down to 25 cm, while SSA was measured at 1 cm depth intervals down to 50 cm. Snow temperature at Dome C has been continuously measured since 2012 at 30-minute intervals. Simulated snow density and SSA were interpolated to a fixed

grid of 1 cm depth resolution and a 24-hour timestep between 1 January 2010 and 1 December 2020, while snow temperature was interpolated onto a 1 mm by 6-hourly grid over the same time period.

330 Density and SSA outputs presented in Fig. 5a and 5b are averaged values over the measurement period. For the most part, the observations fall within the range of the simulations. The simulated SSA profile is consistently within one standard deviation of the measurements below 10cm, above this depth, simulated SSA is overestimated by up to  $10\text{m}^2\text{kg}^{-1}$ . Small standard deviations associated with simulated density and SSA profiles suggest that variability is not well reproduced. As discussed in Libois et al. (2014), the standard version of Crocus is unable to reproduce density and SSA variability with depth due to its one-  
 335 dimensional nature. For the purpose of our study, we consider the standard version sufficient to assess the overall sensitivity of snowpack properties to perturbations in forcings.

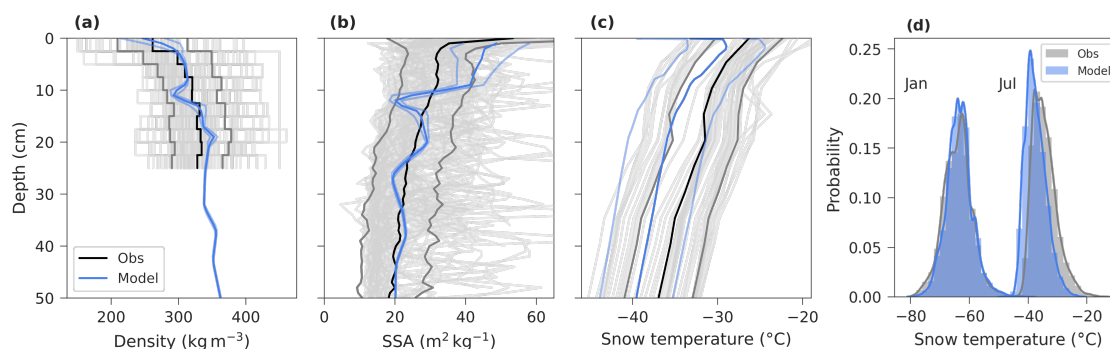


**Figure 5.** Comparison of observations and Crocus simulated snowpack profiles. Density (a) and SSA (b) profiles represent the average from 23 November 2012 and 16 January 2013, covering the measurement period (Libois et al., 2014). Snow temperature profiles (c) both from Crocus (blue) and observations (grey) represent 23 November 2019 to 16 January 2020 averages. Faded grey lines represent individual profiles from observations, and the shaded bands show the standard deviations. Snow temperature distributions in panel (d) represent January and June temperatures between 2016 and 2020.

Snow temperature in Fig. 5c covers the period between 23 November 2019 and 16 January 2020. A  $3^{\circ}\text{C}$  cold bias is apparent, but the mean falls within  $1\sigma$  of the observations. Figure 5d presents distributions of the stacked January snow temperatures between 2016 and 2020, further highlighting this  $3^{\circ}\text{C}$  cold bias during summer ( $-37.1 \pm 3.6^{\circ}\text{C}$  and  $-34.4 \pm 4.1^{\circ}\text{C}$   
 340 for Crocus outputs and observations, respectively). However, winter snow temperatures are well simulated with a 1 m mean of  $-64.7 \pm 4.5^{\circ}\text{C}$  and  $-63.9 \pm 5^{\circ}\text{C}$  from Crocus outputs and observations, respectively. The overestimation of simulated SSA in the top 10cm may be linked to the cold bias in modelled snow temperature during summer via the reduced rate of near-surface snow metamorphism. Alternatively, high SSA may be the result of a recent precipitation event. During large precipitation events, the initial surface snow layer is buried rapidly allowing less time for snow metamorphism (SSA decrease). This is  
 345 particularly pronounced near the surface (top 5 cm) where the majority of metamorphism occurs in response to strong diurnal temperature gradients driven by solar radiation (Picard et al., 2012). This could result in sustained high SSA in the top 10cm.



### 3.2.2 Simulated response of snowpack properties to surface forcing perturbations

Sensitivity tests were run using the Crocus model to assess the response of near-surface snowpack properties to perturbations in surface forcings. The following analysis uses optical radius as a measure of grain size, which is directly linked to SSA and the density of ice (Section 2.3.1), and focuses on the response of near-surface snow density and grain size to the six scenarios outlined in Table 2. We firstly assess the bulk changes in physical properties before looking at the variability with depth.

#### 3.2.3 Bulk snowpack sensitivity

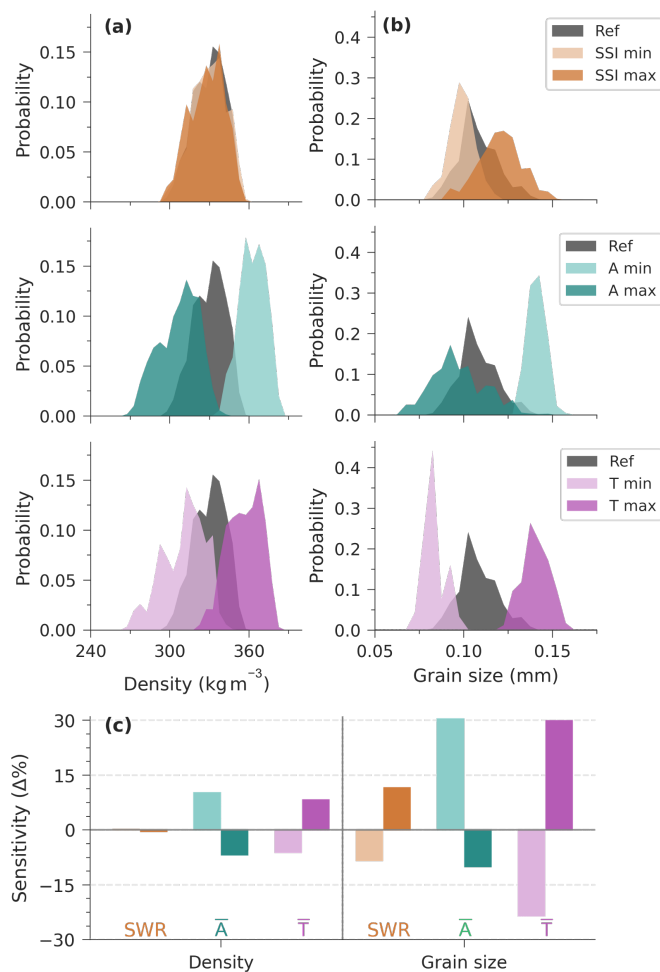


**Figure 6.** Comparison of density and grain size ( $r_{opt}$ ) over the top 20 cm from Crocus sensitivity simulations. Distributions of (a) density and (b) grain size outputs from each test simulation are compared to the reference simulation (bin size is  $5 \text{ kg m}^{-3}$ , and  $0.005 \text{ mm}$ ). In panel (c), bars represent the percentage change in mean density and mean grain size for perturbations in SSI (orange), accumulation rate (green), and temperature (purple); with the decreased scenarios represented by the faded colour, and the increased by the bold colour.

Numerous studies have suggested that modifications in near-surface density and grain size are key parameters influencing elemental fractionation during pore closure (e.g., Bender, 2002; Fujita et al., 2009). Figure 6 shows results from the sensitivity analysis, comparing differences in density and grain size between simulations outlined in Table 2. Overall, grain size is more sensitive to changes in surface forcing than density in the top 20 cm. Perturbations in SSI appear to have minimal influence on density (<1% change compared to the reference simulation) while a 15% decrease in SSI (SSI min) corresponds to an 8% decrease in grain size, and an 11% increase in SSI (SSI max) causes a 12% increase in grain size. The magnitudes of change in both density and grain size are much larger under accumulation rate and temperature perturbations than under SSI perturbations.

Accumulation rate and temperature have opposite effects on density and grain size. A 4°C increase in temperature (T max; 7% increase) increases density and grain size by 8% and 29%, respectively, while increasing the accumulation rate to 4.1 cm yr<sup>-1</sup> (A max; 46% increase) results in a 7% decrease in density and a 10% decrease in grain size. Mean density and grain size respond non-linearly to perturbations in all forcing parameters, as is shown by the magnitude of increase in grain size from decreased accumulation rate being three times greater than the magnitude of decrease induced by an increase in accumulation rate (right panel of Fig. 6c, green bars). This is in line with the dependence of  $\delta O_2/N_2$  to the logarithm of accumulation rate documented in Fig. 3.

### 3.2.4 Depth variability sensitivity

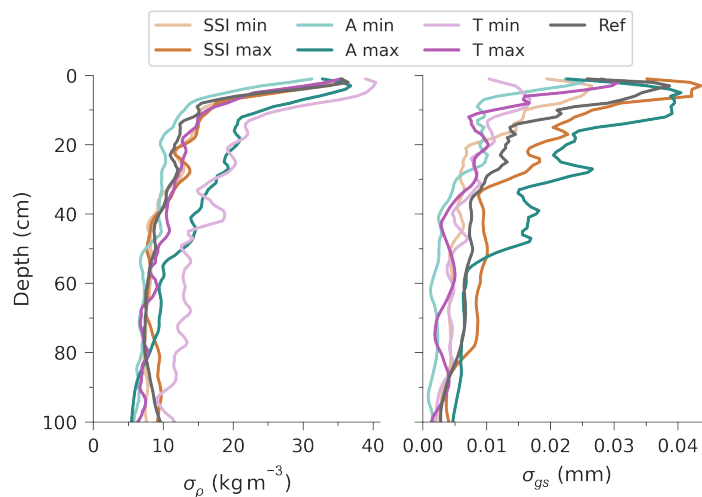


**Figure 7.** Variability in density and grain size with depth over the top 1 m. Each pair of simulations is represented by a colour, SSI in orange, accumulation rate in green, and temperature in purple. The faded line of each pair represents the 800-ka minimum simulation, and the bold line represents the 800-ka maximum simulation.

An alternative (although possibly complementary) explanation for the mechanistic control of snow properties on elemental  
370 fractionation links to stratigraphic layering due to seasonality (Fujita et al., 2009). Here we explore the influence of layering  
by looking at the depth variability in density and grain size as a qualitative measure of stratification (Hörhold et al., 2011),  
assuming that higher variability indicates stronger layering. Variability is defined as the standard deviation of each depth  
interval (denoted  $\sigma$ ) over the period between 1 January 2010 and 1 December 2020.

The  $\sigma$  values for each simulation are presented in Fig. 7 for the top 1 m of snowpack. In all runs,  $\sigma$  peaks near the surface  
375 and decreases with depth for both density and grain size ( $\sigma_\rho$  and  $\sigma_{gs}$ ). Density variability for four out of the six test simulations  
is largely similar to the reference. High-accumulation rate (A max) and low-temperature (T min) are the exception, with an  
increase in  $\sigma_\rho$  of up to  $5 \text{ kg m}^{-3}$  compared to all other runs. The spread in  $\sigma_{gs}$  between simulations is broader than for  $\sigma_\rho$  over  
the top 50 cm, with T min, SSI min, A min, and T max all resulting in reduced variability compared to the reference run.  $\sigma_{gs}$   
increase with an increase in SSI and accumulation rate throughout the top metre. At 100 cm, there is no significant difference  
380 in the  $\sigma_\rho$  and  $\sigma_{gs}$  for the different forcing scenarios, which is discussed in Section 4.4.

To summarise, outputs from the Crocus model indicate that insolation modifies mean grain size but has negligible effect on  
mean density in the top 20 cm. On the other hand, higher air temperature and lower accumulation rate result in increases in  
both mean density and mean grain size, although this change is not necessarily proportional. The depth variability of the two  
snowpack parameters is strongly influenced by increased accumulation rate, with decreased temperature also having a large  
385 effect on density variability, and increased SSI causing an increase in grain size variability.

## 4 Discussion

### 4.1 Evidence for non-SSI dependence of $\delta\text{O}_2/\text{N}_2$

The compilation of deep ice core  $\delta\text{O}_2/\text{N}_2$  records in Fig. 2 reinforces the widely documented anti-correlation between SSI  
and  $\delta\text{O}_2/\text{N}_2$  (e.g. Oyabu et al., 2022; Bouchet et al., 2023). However, a comparison of EDC, Dome F, and South Pole (Fig. 2)  
390 reveals an additional influence of site conditions which cannot be explained by SSI alone. Indeed, our compilation of records  
from 15 sites shows that mean  $\delta\text{O}_2/\text{N}_2$  is strongly correlated with accumulation rate and temperature (Fig. 3). While similar  
spatial and temporal slopes characterise the SSI dependence of  $\delta\text{O}_2/\text{N}_2$ , accumulation rate and temperature appear to be better  
predictors of site mean  $\delta\text{O}_2/\text{N}_2$ . However, a key distinction between the temporal and spatial variations in  $\delta\text{O}_2/\text{N}_2$  lies in the  
range of variations in the three forcing parameters. For example, spatial variations in accumulation rate are much larger than  
395 the variations at a single site through time ( $2\text{--}110 \text{ cm yr}^{-1}$  compared to  $1\text{--}4 \text{ cm yr}^{-1}$  in the EDC core). Conversely, the spatial  
range of SSI values is between  $500\text{--}560 \text{ W m}^{-2}$ , whereas the range at EDC, for instance, is between  $470\text{--}600 \text{ W m}^{-2}$ .

To further constrain the drivers of  $\delta\text{O}_2/\text{N}_2$  variability, we construct a multiple regression to parameterize mean  $\delta\text{O}_2/\text{N}_2$   
as a function of accumulation rate and temperature (Fig. 8). Combined, accumulation rate and temperature can explain up  
to 80% of the total variance in mean  $\delta\text{O}_2/\text{N}_2$  ( $r^2=0.81$ , adjusted  $r^2=0.766$ ). Including SSI to the multiple linear regression  
400 further improves the adjusted  $r^2$  from 0.77 to 0.82. These results reiterate that  $\delta\text{O}_2/\text{N}_2$  is highly sensitive to accumulation  
rate, especially at low accumulation sites. Although not explicitly explored, the site dependence of  $\delta\text{O}_2/\text{N}_2$  has been noted in

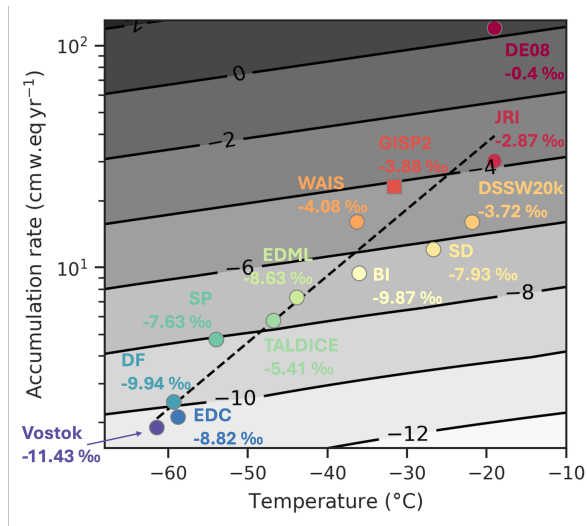


**Figure 8.**  $\delta\text{O}_2/\text{N}_2$  as a function of accumulation rate and temperature. Contours show the predicted  $\delta\text{O}_2/\text{N}_2$  values calculated using the multiple linear regression of accumulation rate (A) and temperature (T) ( $\delta\text{O}_2/\text{N}_2 = -0.03 \cdot T + 2.96 \cdot \log(A) - 14.6$ ). Measured mean  $\delta\text{O}_2/\text{N}_2$  values are noted alongside each site. The accumulation rate-temperature regression (dashed, black line) is defined using a regression on temperature and accumulation rate for all sites in the data compilation ( $A = \exp^{((0.069 \cdot T) + 4.98)}$ ).

previous studies. For example, Bazin et al. (2016) identified an offset in absolute  $\delta\text{O}_2/\text{N}_2$  values in the Vostok core compared to Dome F and EDC, similar to our observation in Fig. 2. By including records from numerous ice cores we are able to definitively show that absolute values are systematically linked to site accumulation rate and temperature.

#### 405 4.2 Millennial scale variability in $\delta\text{O}_2/\text{N}_2$ records

Further investigation into drivers of  $\delta\text{O}_2/\text{N}_2$  variability in the EDC core reveals a millennial-scale climate signal in the  $\delta\text{O}_2/\text{N}_2$  record. The timing of these anomalies in  $\delta\text{O}_2/\text{N}_2$  broadly correspond to those in the  $\delta\text{D}$  record from EDC between 200–260 ka BP (Fig. 4), suggesting that millennial-scale variations can arise from changes in accumulation rate and/or temperature. The anomalies observed in the EDC  $\delta\text{O}_2/\text{N}_2$  record are not unique to this period but vary between time periods and sites  
 410 (Supplement S2). Indeed, a similar effect was previously observed in the GISP2 core, where  $\delta\text{O}_2/\text{N}_2$  was found to be positively correlated with local temperature over millennial timescales (i.e., Dansgaard-Oeschger (D-O) events) (Suwa and Bender, 2008b).

Previous studies suggest an overlap between the drivers of  $\delta\text{O}_2/\text{N}_2$  variability and those of total air content (TAC) variability (Fujita et al., 2009; Lipenkov et al., 2011). Ice core  $\delta\text{O}_2/\text{N}_2$  and TAC records exhibit slight differences in their spectral signals,  
 415 whereby  $\delta\text{O}_2/\text{N}_2$  is dominated by precession (hence SSI pacing), whereas TAC is dominated by obliquity (hence the integrated summer insolation pacing). However, variability in both records are linked to local insolation via the modulation of near-surface snow properties, which ultimately influence pore closure processes (Lipenkov et al., 2011). Fujita et al. (2009) hypothesised

that permeation, the process driving size-dependent fractionation of  $\delta\text{O}_2/\text{N}_2$ , can explain about half the variation in TAC, with the rest being driven by effusion (not believed to substantially influence  $\delta\text{O}_2/\text{N}_2$ ). We therefore draw on TAC studies to aid our interpretation of millennial-scale variability in  $\delta\text{O}_2/\text{N}_2$ .

Several mechanisms have been proposed to explain millennial-scale variability in TAC and  $\delta\text{O}_2/\text{N}_2$ , with apparent differences in the dominant mechanisms between hemispheres; TAC is anti-correlated with accumulation rate in the NGRIP core (Eicher et al., 2016) but positively correlated in the South Pole ice core (Epifanio et al., 2023). Eicher et al. (2016) attributed this anti-correlation between TAC and accumulation rate during D-O events at NGRIP, Greenland, to transient effects in the firn column. During the initial stage of a D-O event, rapid increases in accumulation rate increase overburden pressure, reducing the pore volume at close off, and consequently decreasing TAC (Eicher et al., 2016). Similarly, Kobashi et al. (2015) suggested that rapid changes in overburden pressure could explain the negative correlation between  $\delta\text{Ar}/\text{N}_2$  (and thus,  $\delta\text{O}_2/\text{N}_2$ ) and accumulation rate over multi-decadal timescales at GISP2 via its influence on the permeation rate of gases in the deep firn. In contrast, a positive correlation between TAC and accumulation rate at South Pole is attributed to increased snow burial rates, leading to smaller grains and therefore increased pore volume at close-off (Epifanio et al., 2023). Such a grain size mechanism is understood to drive the integrated summer insolation signal in TAC records (Raynaud et al., 2007) as well as the SSI signal in  $\delta\text{O}_2/\text{N}_2$  records (e.g. Bender, 2002).

Transient effects in the firn column in response to rapid climatic changes (linked to overburden pressure) are expected to be largely absent from Antarctic sites due to reduced magnitude in climate variability compared to Greenland. However, an accumulation-dependent grain size mechanism may explain the positive correlation between  $\delta\text{D}$  and  $\delta\text{O}_2/\text{N}_2$  at EDC. Epifanio et al. (2023) proposed that the contradictory behaviour of TAC between NGRIP and South Pole may be explained by varying responses of the firn to changes in accumulation rate depending site surface climate conditions. They suggest that a grain size mechanism dominates TAC modulation at low accumulation sites while transient effects from rapid climatic changes are more important at warm, high accumulation sites. We expect that the mechanisms driving  $\delta\text{O}_2/\text{N}_2$  are also modulated by accumulation rate. Indeed, observations of  $\delta\text{O}_2/\text{N}_2$  records from South Pole appear to support the in-phase coherence between  $\delta\text{O}_2/\text{N}_2$  and  $\delta\text{D}$  in the EDC core, but only when  $\delta\text{D}$  is sufficiently low (Fig. S4 in Supplement). A shifted, anti-phase relationship is apparent when  $\delta\text{D}$  is higher, which suggests that different mechanisms may be dominant under high accumulation conditions.

### 4.3 Towards a mechanistic understanding of $\delta\text{O}_2/\text{N}_2$ variability at low-accumulation sites

Previous studies have demonstrated the link between climate and snow metamorphism, showing that snow metamorphism is enhanced during summers with very low accumulation rates (Picard et al., 2012; Casado et al., 2021). However, the connection to pore closure processes has received less attention. One possible reason for this gap is the added complexity which would be required to implement surface snow metamorphism into firn models, which necessitates prior information such as surface grain size. The following sections propose some ideas to bridge this gap by examining the influence of local climate parameters (accumulation rate and temperature) and SSI on near-surface snow metamorphism, and how these might modulate elemental fractionation during pore closure.

### 4.3.1 Surface snow properties

Variations in grain properties are thought to drive the SSI signal in  $\delta\text{O}_2/\text{N}_2$  records (e.g., Bender, 2002; Fujita et al., 2009). Indeed, results from sensitivity tests in Fig. 6 show an increase in grain size under increased SSI, which is attributed to both  
455 stronger near-surface temperature gradients (Appendix B in Vionnet et al., 2012) and higher snow temperatures during summer (Fig. S4 in Supplement). Negligible change in simulated density under perturbations in SSI appears to support the hypothesis of a near-surface grain size mechanism (e.g., Bender, 2002), although this may be linked to the absence of vapour transport in the Crocus model. Increased snow metamorphism rate can also explain the increased grain size with increased temperature (Legagneux et al., 2003), while an increase in density results from increased compaction rates (Vionnet et al., 2012). The  
460 decrease in grain size with increased accumulation rate is the result of shorter residence time of a snow layer in the upper centimetres to metres of the snowpack, where temperature gradients are strongest (Picard et al., 2012).

It is widely accepted that permeation is the process by which small molecules escape during pore closure (e.g., Ikeda-Fukazawa et al., 2004; Huber et al., 2006; Severinghaus and Battle, 2006). Gregory et al. (2014) found that permeability is increased in high-density, large-grained firn due to a less complex pore structure. Indeed, Calonne et al. (2022) showed that  
465 grain size has a strong influence on permeability, such that for a given density, permeability is increased with grain size. Our results show that high SSI and low accumulation rate are associated with larger grain size and lower  $\delta\text{O}_2/\text{N}_2$ . This observation supports the hypothesis that increased SSI (decreased accumulation rate) ultimately leads to lower  $\delta\text{O}_2/\text{N}_2$  due to the increased permeability associated with increased grain size (e.g., Severinghaus and Battle, 2006; Fujita et al., 2009), and suggests a similar mechanism may partially explain the accumulation rate dependence.

470 Identifying the mechanisms driving the accumulation rate dependence of  $\delta\text{O}_2/\text{N}_2$  is complicated by the fact that, at polar sites, accumulation rate tends to covary with temperature (Fig. 8). Thus, an increase in grain size with increased near-surface residence time (decreased accumulation rate) will be countered by reduced snow metamorphism rates with a decrease in temperature (Fig. 6). These counteracting effects were invoked by Kawamura et al. (2007) to explain the absence of a 100-kyr periodicity in  $\delta\text{O}_2/\text{N}_2$  records at Dome Fuji. However, a stronger correlation between  $\delta\text{O}_2/\text{N}_2$  and accumulation rate than  
475 temperature in Fig. 3 suggests a dominant role of accumulation. Therefore, we propose that a grain size mechanism controlling pore structure at close-off, like that of SSI, may explain the positive correlation between accumulation rate and  $\delta\text{O}_2/\text{N}_2$  in the EDC core (Fig. 3b).

Previous studies propose that firn column characteristics, such as delta-age, will also modulate  $\delta\text{O}_2/\text{N}_2$  via changes in accumulation rate and temperature (Severinghaus and Battle, 2006; Bazin et al., 2016). One mechanism links to the time  
480 for pores to close off. At low accumulation sites, pores will take longer to fully close, and thus, experience more elemental fractionation (Severinghaus and Battle, 2006). Additional hypotheses point to LIZ thickness and pore space geometry (or tortuosity) (e.g., Fujita et al., 2009). Low accumulation sites tend to have thinner LIZs (e.g., Landais et al., 2006; Witrant et al., 2012) and less tortuous pore structure in deep firn associated with large, rounded grains (Gregory et al., 2014). Such characteristics are associated with increased gas diffusivity that would facilitate the removal of  $\text{O}_2$ -enriched gas back to the  
485 atmosphere. In contrast, at high accumulation sites, the associated decrease in gas diffusivity in the LIZ would lead to a build

up of a stagnant air enriched in  $O_2$  resulting in the trapping of gas with relatively high  $\delta O_2/N_2$ . Alternatively, Hutterli et al. (2009) proposed that varying near-surface temperature gradients under different SSI intensities modulate anisotropy of the snow leading to vertically elongated pores (as was confirmed by Leinss et al. (2020)) under high SSI (low accumulation) conditions. They argue that elongated pores facilitate vertical diffusivity in the LIZ, leading to greater fractionation of  $\delta O_2/N_2$  (Hutterli et al., 2009), an alternative but complimentary mechanism to LIZ thickness. A simplified and non-exhaustive illustration of these various interactions can be found in Fig. S6 in the Supplement.

The aforementioned mechanisms relating to firn column characteristics indicate a positive correlation between  $\delta O_2/N_2$  and accumulation rate. This is consistent with Fig. 3b but cannot be directly supported by our sensitivity results. Based on the sensitivity tests in Fig. 6, a link to surface density is not clear. We expect that the role of density in modulating  $\delta O_2/N_2$  derives from the grain size dependence of densification rates invoked by Freitag et al. (2004), providing an additional link between near-surface grain size and  $\delta O_2/N_2$ , as is outlined in the following section.

### 4.3.2 Depth-dependent variability as a proxy for layering

Density stratification in deep firn has also been invoked to modulate  $\delta O_2/N_2$  (Fujita et al., 2009). Results from the Crocus model are tentatively used to infer the sensitivity of near-surface density and grain size variability to perturbations in input forcing parameters. Figure 7 shows that grain size variability is increased with an increase in both SSI and accumulation rate. For SSI, this is expected given enhanced snow metamorphism during summer due to higher snow temperatures while winter conditions are largely unchanged (Fig. S5 in Supplement). Decreased grain size variability in both the increased and decreased temperature simulations is likely linked to the way in which temperature forcing is perturbed. By applying a constant increase in air temperature, the strength of metamorphism is increased during winter due to higher temperatures (Legagneux et al., 2003; Flanner and Zender, 2006), but largely unchanged during summer due to the dominant influence of insolation on summer snow temperature (Fig. S5), resulting in homogeneity within the snowpack.

Linking variability near the surface with variability in deep firn is not trivial. Indeed, a study by Hörhold et al. (2011) used a compilation of firn cores from numerous polar sites to show that density variability in deep firn is positively correlated with local accumulation rate and temperature, but anti-correlated with near-surface density variability. However, this anti-correlation was not observed by Inoue et al. (2023) when comparing firn cores in the Dome Fuji area. Additional consideration, both from data and modelling approaches, is required for density inversions in the firn column – whereby relatively low-density layers in the upper part of the firn become relatively high-density layers below the density inversion depth, due to preferential deformation in the upper firn (Freitag et al., 2004; Fujita et al., 2009). Freitag et al. (2004) proposed that the inversion is largely driven by grain size, such that initially low-density layers associated with large grain size become relatively high-density layers with large grain size below the density inversion. This has since been supported by Gregory et al. (2014) who further show that near surface grain size determines the density at which pores close-off. They show that large-grained, high-density layers are more permeable and hence, close off deeper than fine-grained, low-density layers. In addition, Hörhold et al. (2012) suggested that stratification at depth is influenced by impurity content, with impurity-rich layers being more susceptible to densification. Given the array of factors proposed to influence deep firn density variability, we focus on the role of grain size variability.

520 No inversion is observed for grain size variability. Deep firn layers retain evidence of near-surface grain size, which is determined by snow metamorphism and accumulation rate (Gregory et al., 2014), as mentioned previously. While our sensitivity tests are constrained to the near surface, we draw on previous studies to suggest potential links with deep firn properties and  $\delta\text{O}_2/\text{N}_2$  fractionation. Given the presence of a density inversion at Dome C (Hörhold et al., 2011), we may expect that relatively increased variability in near-surface grain size from our sensitivity tests would translate to increased grain size and  
525 density variability in the deep firn. As such, increased grain size variability in our SSI max simulation (Fig. 7) supports the conclusions of Fujita et al. (2009), that elemental fractionation is enhanced under high SSI conditions due partially to layering.

The link to accumulation rate is less clear. As for SSI, we observe an increase in grain size variability with increased accumulation rate. However, according to the layering hypothesis, this should result in more  $\delta\text{O}_2/\text{N}_2$  fractionation at close off, which contradicts our observations of a positive correlation between  $\delta\text{O}_2/\text{N}_2$  and accumulation rate (Fig. 3b). Instead,  
530 our observations suggest that a decrease in mean grain size with increased accumulation rate is dominant over the layering effect. Future work would benefit from an inter site comparison of deep firn properties alongside gas measurements in order to disentangle these effects.

Extracting concrete conclusions from our variability analysis and extrapolating these into the deep firn is inhibited by both the ascribed forcing perturbations and the aggregation scheme of the model, which is particularly sensitive to changes in  
535 accumulation rate. We thus conclude that the simulations performed with the Crocus model can support a mechanism linked to average grain size on  $\delta\text{O}_2/\text{N}_2$  but not a mechanism implying density or grain size variability. However, our conclusion does not rule out the effect of layering or grain size variability on  $\delta\text{O}_2/\text{N}_2$  variability but highlights a limitation in our study, as explained in the next section.

#### 4.4 Limitations and perspectives

540 A number of limitations have been mentioned throughout our study and warrant some further discussion. As mentioned in Section 4.3.2, our study is unable to fully consider the sensitivity of layering to perturbations in forcing parameters. Firstly, near-surface density and grain size variability are not fully captured by the model which can be partially attributed to the absence of snow transport by the wind in the standard version of Crocus (Libois et al., 2014). While wind is known to strongly influence snow properties (e.g. Inoue et al., 2023), we are limited in our understanding of winds throughout the past 800 kyr  
545 and therefore wind effects are not considered in our study. Secondly, the aggregation of layers with depth in Crocus make it difficult to focus on both the fine-layered near-surface snow, and the propagation of stratified layers into the deep firn. Accurate assessment of the layering effect would require a new dedicated snow model preserving individual snow layers and properties over a large depth range, from the surface to LIZ, and at high resolution.

While the single-parameter sensitivity tests presented here provide useful insights for understanding physical mechanisms,  
550 they do not account for complex compound effects associated with the covariance of accumulation rate and temperature at polar sites. Additional tests perturbing both accumulation rate and temperature simultaneously indicate that snowpack properties are very sensitive to the ascribed accumulation rate and temperature values i.e., for glacial temperature reconstructions which are debated to have been overestimated by as much as 5°C at Dome C (Buizert et al., 2021). Moreover, the additive



effects from the single-parameter sensitivity tests for accumulation rate and temperature do not equal the effects of multi-  
555 parameter sensitivity simulations (i.e., perturbing both accumulation rate and temperature). This discrepancy highlights the  
complex interactions between quasi-covarying accumulation rate and temperature on snow properties. Indeed, a cancellation  
of the accumulation rate and temperature effects were invoked by Kawamura et al. (2007) to explain the absence of a 100-ka  
periodicity in  $\delta\text{O}_2/\text{N}_2$  at Dome Fuji. Given the uncertainties in climate reconstructions and the limitations of the model, we  
refrained from using multi-parameter simulations for interpretation of empirical results. Future studies would benefit from ob-  
560 taining  $\delta\text{O}_2/\text{N}_2$  measurements in open and closed porosity at sites with distinct characteristics to better constrain the physical  
mechanisms.

Finally, given that the high resolution  $\delta\text{O}_2/\text{N}_2$  records tend to be from Antarctic sites (e.g., Fig. 2), our study is slightly  
biased towards low accumulation conditions. Indeed, initial temporal analysis of  $\delta\text{O}_2/\text{N}_2$  variability at South Pole suggests  
that different mechanisms may be dominant at relatively high accumulation sites, as has been previously suggested (Suwa  
565 and Bender, 2008b; Kobashi et al., 2015), but was outside the scope of this study. Future studies focusing on the dominance  
of different mechanisms under different site conditions would therefore benefit from obtaining high resolution measurements  
from sites with distinct characteristics. Furthermore, a comparison of deep firn properties alongside  $\delta\text{O}_2/\text{N}_2$  measurements  
from the open and closed porosity would aid a mechanistic understanding.

## 5 Conclusions

570 We present a compilation of  $\delta\text{O}_2/\text{N}_2$  records measured on multiple ice cores from Antarctica and Greenland to develop a  
mechanistic understanding of  $\delta\text{O}_2/\text{N}_2$  variability. Analysis of both temporal (single-site) and spatial (multi-site) variability  
in  $\delta\text{O}_2/\text{N}_2$  presents new evidence of a dependence on local climate (accumulation rate and temperature), in addition to the  
well-documented SSI dependence. High resolution measurements from the EDC ice core reveals millennial-scale variability  
in  $\delta\text{O}_2/\text{N}_2$  in-phase with  $\delta\text{D}$  records when both parameters are plotted on the AICC2023 ice-age scale. The inter-site analysis  
575 showed an increase in mean  $\delta\text{O}_2/\text{N}_2$  for sites with higher accumulation rate and temperature, which is analogous with the  
temporal analysis from EDC showing  $\delta\text{O}_2/\text{N}_2$  to increase together with  $\delta\text{D}$ .

We suggest that a mechanism relating to firn physical properties can partially explain both the influence of SSI and local  
climate on  $\delta\text{O}_2/\text{N}_2$  variability. Sensitivity tests using the Crocus model show that grain size is very responsive to perturbations  
in SSI, accumulation rate and air temperature, while density responds to all but SSI perturbations. Our findings support the  
580 hypothesis that a grain size mechanism is a dominant driver of elemental fractionation at low accumulation sites, such that  
increased grain size for a given density facilitates  $\text{O}_2$  expulsion via enhanced permeability. Furthermore, our results support  
the hypothesis that the presence, or lack thereof, of a local climatic signal in  $\delta\text{O}_2/\text{N}_2$  variability is due to the delicate balance  
between the counter-effects of accumulation rate and temperature on grain properties. However, the inter-site results suggest  
that low accumulation, low temperature sites experience stronger elemental fractionation, having a comparable effect to high  
585 insolation.

While our findings from the  $\delta\text{O}_2/\text{N}_2$  data compilation are supported by the Crocus sensitivity tests, we acknowledge that additional mechanisms are at play. In particular, the influence of deep firn layering – itself linked to surface snow metamorphism – could not be tested fully in this study but is believed to play a major role in modulating  $\delta\text{O}_2/\text{N}_2$ . Determining the relative influence of stratification, firn physical properties, and residence time in the lock-in zone using a combination of firn models and observations would be useful for future studies.

*Code availability.* The Crocus model is open-source, and the code is available at [https://opensource.umr-cnrm.fr/projects/snowtools\\_git/wiki/Procedure\\_for\\_new\\_users](https://opensource.umr-cnrm.fr/projects/snowtools_git/wiki/Procedure_for_new_users). The version used is labeled as Surfex V8\_1.

*Data availability.* Published accumulation rate and temperature reconstructions used for the data compilation will be accessible at <https://10.5281/zenodo.12571888>. All published and unpublished  $\delta\text{O}_2/\text{N}_2$  datasets measured at LSCE are also available at this link.

*Author contributions.* AL, EC and FP performed measurements/produced the unpublished datasets measured at LSCE - on ice provided by RM and BS - and CB and JS provided unpublished datasets measured at Scripps. Snow temperature data from Dome C was acquired and shared by LA and GP. RHS ran the Crocus simulations, with the support of MD and QL. RHS and AL prepared the manuscript with contributions from all co-authors.

*Competing interests.* At least one of the authors is a member of the editorial board of The Cryosphere.

*Acknowledgements.* This publication was generated in the frame of DEEPICE project. The project has received funding from the European Union's Horizon 2020 research and innovation programme under the Marie Skłodowska-Curie grant agreement No 955750. The measurements leading to these results has also received funding from the European Union's H2020 Programme (H2020/20192024)/ERC grant agreement no. 817493 (ERC ICORDA). EC acknowledges the financial support from the French National Research Agency under the "Programme d'Investissements d'Avenir" (ANR-19-MPGA-0001). MD has received funding from the European Research Council (ERC) under the European Union's Horizon 2020 research and innovation program (IVORI; grant no. 949516). We also thank Matthieu Fructus for providing his expertise and support in the Crocus model.

*Financial support.* This research has been supported by the Horizon 2020 research and innovation programme (grant no. 955750 and grant no. 817493).

## References

- 610 Albert, M., Shuman, C., Courville, Z., Bauer, R., Fahnestock, M., and Scambos, T.: Extreme firn metamorphism: impact of decades of vapor transport on near-surface firn at a low-accumulation glazed site on the East Antarctic plateau, *Annals of Glaciology*, 39, 73–78, <https://doi.org/10.3189/172756404781814041>, 2004.
- Alley, R. B. and Koci, B. R.: Ice-core analysis at site A, Greenland: preliminary results, *Annals of Glaciology*, 10, 1–4, <https://doi.org/10.3189/S0260305500004067>, 1988.
- 615 Alley, R. B., Meese, D., Shuman, C., Gow, A., Taylor, K., Grootes, P., White, J., Ram, M., Waddington, E., Mayewski, P., et al.: Abrupt increase in Greenland snow accumulation at the end of the Younger Dryas event, *Nature*, 362, 527–529, <https://doi.org/10.1038/362527a0>, 1993.
- Battle, M., Bender, M., Sowers, T., Tans, P., Butler, J., Elkins, J., Ellis, J., Conway, T., Zhang, N., Lang, P., et al.: Atmospheric gas concentrations over the past century measured in air from firn at the South Pole, *Nature*, 383, 231–235, <https://doi.org/10.1038/383231a0>,  
620 1996.
- Battle, M., Severinghaus, J., Sofen, E., Plotkin, D., Orsi, A., Aydin, M., Montzka, S., Sowers, T., and Tans, P.: Controls on the movement and composition of firn air at the West Antarctic Ice Sheet Divide, *Atmospheric Chemistry and Physics*, 11, 11 007–11 021, <https://doi.org/10.5194/acp-11-11007-2011>, 2011.
- Bazin, L., Landais, A., Lemieux-Dudon, B., Toyé Mahamadou Kele, H., Veres, D., Parrenin, F., Martinerie, P., Ritz, C., Capron, E., Lipenkov,  
625 V., Loutre, M.-F., Raynaud, D., Vinther, B., Svensson, A., Rasmussen, S. O., Severi, M., Blunier, T., Leuenberger, M., Fischer, H., Masson-Delmotte, V., Chappellaz, J., and Wolff, E.: An optimized multi-proxy, multi-site Antarctic ice and gas orbital chronology (AICC2012): 120–800 ka, *Climate of the Past*, 9, 1715–1731, <https://doi.org/10.5194/cp-9-1715-2013>, 2013.
- Bazin, L., Landais, A., Capron, E., Masson-Delmotte, V., Ritz, C., Picard, G., Jouzel, J., Dumont, M., Leuenberger, M., and Prié, F.: Phase relationships between orbital forcing and the composition of air trapped in Antarctic ice cores, *Climate of the Past*, 12, 729–748,  
630 <https://doi.org/10.5194/cp-12-729-2016>, 2016.
- Bender, M., Sowers, T., and Lipenkov, V.: On the concentrations of O<sub>2</sub>, N<sub>2</sub>, and Ar in trapped gases from ice cores, *Journal of Geophysical Research: Atmospheres*, 100, 18 651–18 660, <https://doi.org/10.1029/94JD02212>, 1995.
- Bender, M. L.: Orbital tuning chronology for the Vostok climate record supported by trapped gas composition, *Earth and Planetary Science Letters*, 204, 275–289, [https://doi.org/https://doi.org/10.1016/S0012-821X\(02\)00980-9](https://doi.org/https://doi.org/10.1016/S0012-821X(02)00980-9), 2002.
- 635 Bender, M. L., Tans, P. P., Ellis, J., Orchard, J., and Habfast, K.: A high precision isotope ratio mass spectrometry method for measuring the O<sub>2</sub>/N<sub>2</sub> ratio of air, *Geochimica et Cosmochimica Acta*, 58, 4751–4758, [https://doi.org/https://doi.org/10.1016/0016-7037\(94\)90205-4](https://doi.org/https://doi.org/10.1016/0016-7037(94)90205-4), 1994.
- Bertler, N. A., Conway, H., Dahl-Jensen, D., Emanuelsson, U., Winstrup, M., Vallelonga, P. T., Lee, J. E., Brook, E. J., Severinghaus, J. P., Fudge, T. J., Keller, E. D., Baisden, W. T., Hindmarsh, R. C. A., Neff, P. D., Blunier, T., Edwards, R. L., Mayewski, P. A., Kipfstuhl, S., Buizert, C., Canessa, S., Dacic, R., Kjær, H. A., Kurbatov, A., Zhang, D., Waddington, E. D., Baccolo, G., Beers, T., Brightley, H. J., Carter, L., Clemens-Sewall, D., Ciobanu, V. G., Delmonte, B., Eling, L., Ellis, A. A., Ganesh, S., Golledge, N. R., Haines, S. A., Handley, M., Hawley, R. L., Hogan, C. M., Johnson, K. M., Korotkikh, E., Lowry, D. P., Mandeno, D., McKay, R. M., Menking, J. A., Naish, T. R., Noerling, C., Ollive, A., Orsi, A. J., Proemse, B. C., Pyne, A. R., Pyne, R. L., Renwick, J., Scherer, R. P., Semper, S., Simonsen, M., Sneed, S. B., Steig, E. J., Tuohy, A., Ulayottil Venugopal, A., Valero Delgado, F., Venkatesh, J., Wang, F., Wang, S.,  
645 Winski, D. A., Winton, V. H. L., Whiteford, A., Xiao, C., Yang, J., and Zhang, X.: Roosevelt Island Climate Evolution (RICE) ice core

- isotope record, <https://doi.org/10.1594/PANGAEA.880396>, supplement to: Bertler, NA et al. (2018): The Ross Sea dipole - temperature, snow accumulation and sea ice variability in the Ross Sea region, Antarctica, over the past 2700 years. *Climate of the Past*, 14, 193-214, <https://doi.org/10.5194/cp-14-193-2018>, 2017.
- 650 Bouchet, M., Landais, A., Grisart, A., Parrenin, F., Prié, F., Jacob, R., Fourré, E., Capron, E., Raynaud, D., Lipenkov, V. Y., Loutre, M.-F., Extier, T., Svensson, A., Legrain, E., Martinerie, P., Leuenberger, M., Jiang, W., Ritterbusch, F., Lu, Z.-T., and Yang, G.-M.: The Antarctic Ice Core Chronology 2023 (AICC2023) chronological framework and associated timescale for the European Project for Ice Coring in Antarctica (EPICA) Dome C ice core, *Climate of the Past*, 19, 2257–2286, <https://doi.org/10.5194/cp-19-2257-2023>, 2023.
- 655 Bouchet, M., Landais, A., Grisart, A., Parrenin, F., Prié, F., Jacob, R., Fourré, E., Capron, E., Raynaud, D., Lipenkov, V. Y., Loutre, M.-F., Extier, T., Svensson, A. M., Martinerie, P., Leuenberger, M. C., Jiang, W., Ritterbusch, F., Lu, Z.-T., and Yang, G.-M.: AICC2023, VOSTOK, PANGAEA, <https://doi.org/10.1594/PANGAEA.961022>, in: Bouchet, M et al. (2023): The Antarctic ice core chronology (AICC2023) [dataset bundled publication]. PANGAEA, <https://doi.org/10.1594/PANGAEA.961017>, 2023.
- Buiron, D., Chappellaz, J., Stenni, B., Frezzotti, M., Baumgartner, M., Capron, E., Landais, A., Lemieux-Dudon, B., Masson-Delmotte, V., Montagnat, M., et al.: TALDICE-1 age scale of the Talos Dome deep ice core, East Antarctica, *Climate of the Past*, 7, 1–16, <https://doi.org/10.5194/cp-7-1-2011>, 2011.
- 660 Buizert, C.: The Ice Core Gas Age-Ice Age Difference as a Proxy for Surface Temperature, *Geophysical Research Letters*, 48, e2021GL094241, <https://doi.org/10.1029/2021GL094241>, 2021.
- Buizert, C. and Severinghaus, J. P.: Dispersion in deep polar firn driven by synoptic-scale surface pressure variability, *The Cryosphere*, 10, 2099–2111, <https://doi.org/10.5194/tc-10-2099-2016>, 2016.
- Buizert, C., Martinerie, P., Petrenko, V., Severinghaus, J., Trudinger, C., Witrant, E., Rosen, J., Orsi, A., Rubino, M., Etheridge, D., et al.: Gas 665 transport in firn: multiple-tracer characterisation and model intercomparison for NEEM, Northern Greenland, *Atmospheric Chemistry and Physics*, 12, 4259–4277, <https://doi.org/10.5194/acp-12-4259-2012>, 2012.
- Buizert, C., Baggenstos, D., Bereiter, B., Bertler, N., Brook, E. J., and Etheridge, D.: Multi-site ice core Krypton stable isotope ratios, <https://doi.org/10.15784/601394>, 2020.
- 670 Buizert, C., Fudge, T., Roberts, W. H., Steig, E. J., Sherriff-Tadano, S., Ritz, C., Lefebvre, E., Edwards, J., Kawamura, K., Oyabu, I., et al.: Antarctic surface temperature and elevation during the Last Glacial Maximum, *Science*, 372, 1097–1101, <https://doi.org/10.1126/science.abd2897>, 2021.
- Buizert, C., Shackleton, S., Severinghaus, J. P., Roberts, W. H. G., Seltzer, A., Bereiter, B., Kawamura, K., Baggenstos, D., Orsi, A. J., Oyabu, I., Birner, B., Morgan, J. D., Brook, E. J., Etheridge, D. M., Thornton, D., Bertler, N., Pyne, R. L., Mulvaney, R., Mosley-Thompson, E., Neff, P. D., and Petrenko, V. V.: The new Kr-86 excess ice core proxy for synoptic activity: West Antarctic storminess 675 possibly linked to Intertropical Convergence Zone (ITCZ) movement through the last deglaciation, *Climate of the Past*, 19, 579–606, <https://doi.org/10.5194/cp-19-579-2023>, 2023.
- Calonne, N., Burr, A., Philip, A., Flin, F., and Geindreau, C.: Effective coefficient of diffusion and permeability of firn at Dome C and Lock In, Antarctica, and of various snow types – estimates over the 100–850 kg m<sup>-3</sup> density range, *The Cryosphere*, 16, 967–980, <https://doi.org/10.5194/tc-16-967-2022>, 2022.
- 680 Capron, E., Landais, A., Buiron, D., Cauquoin, A., Chappellaz, J., Debret, M., Jouzel, J., Leuenberger, M., Martinerie, P., Masson-Delmotte, V., Mulvaney, R., Parrenin, F., and Prié, F.: Glacial–interglacial dynamics of Antarctic firn columns: comparison between simulations and ice core air-delta;<sup>15</sup>N measurements, *Climate of the Past*, 9, 983–999, <https://doi.org/10.5194/cp-9-983-2013>, 2013.

- Carmagnola, C., Morin, S., Lafaysse, M., Domine, F., Lesaffre, B., Lejeune, Y., Picard, G., and Arnaud, L.: Implementation and evaluation of prognostic representations of the optical diameter of snow in the SURFEX/ISBA-Crocus detailed snowpack model, *The Cryosphere*, 8, 417–437, <https://doi.org/10.5194/tc-8-417-2014>, 2014.
- Casado, M., Landais, A., Picard, G., Arnaud, L., Dreossi, G., Stenni, B., and Prié, F.: Water Isotopic Signature of Surface Snow Metamorphism in Antarctica, *Geophysical Research Letters*, 48, e2021GL093382, <https://doi.org/https://doi.org/10.1029/2021GL093382>, 2021.
- Champollion, N., Picard, G., Arnaud, L., Lefebvre, E., Macelloni, G., Rémy, F., and Fily, M.: Marked decrease in the near-surface snow density retrieved by AMSR-E satellite at Dome C, Antarctica, between 2002 and 2011, *The Cryosphere*, 13, 1215–1232, <https://doi.org/10.5194/tc-13-1215-2019>, 2019.
- Clow, G. D.: GISP2-D Temperature, <https://doi.org/10.1594/PANGAEA.55517>, 1999.
- Crotti, I., Landais, A., Stenni, B., Bazin, L., Parrenin, F., Frezzotti, M., Ritterbusch, F., Lu, Z.-T., Jiang, W., Yang, G.-M., et al.: An extension of the TALDICE ice core age scale reaching back to MIS 10.1, *Quaternary Science Reviews*, 266, 107078, <https://doi.org/10.1016/j.quascirev.2021.107078>, 2021.
- Cuffey, K. M. and Clow, G. D.: GISP2 accumulation rate history, <https://doi.org/10.1594/PANGAEA.56075>, 1999.
- Cuffey, K. M. and Paterson, W. S. B.: *The physics of glaciers*, Academic Press, 2010.
- Domine, F., Salvatori, R., Legagneux, L., Salzano, R., Fily, M., and Casacchia, R.: Correlation between the specific surface area and the short wave infrared (SWIR) reflectance of snow, *Cold Regions Science and Technology*, 46, 60–68, <https://doi.org/https://doi.org/10.1016/j.coldregions.2006.06.002>, 2006.
- Eicher, O., Baumgartner, M., Schilt, A., Schmitt, J., Schwander, J., Stocker, T. F., and Fischer, H.: Climatic and insolation control on the high-resolution total air content in the NGRIP ice core, *Climate of the Past*, 12, 1979–1993, <https://doi.org/10.5194/cp-12-1979-2016>, 2016.
- EPICA community members: Eight glacial cycles from an Antarctic ice core, *Nature*, 429, 623–628, <https://doi.org/10.1038/nature02599>, 2004.
- EPICA community members: One-to-one coupling of glacial climate variability in Greenland and Antarctica, *Nature*, 444, 195–198, <https://doi.org/10.1038/nature05301>, 2006.
- Epifanio, J. A., Brook, E. J., Buizert, C., Pettit, E. C., Edwards, J. S., Fegyveresi, J. M., Sowers, T. A., Severinghaus, J. P., and Kahle, E. C.: Millennial and orbital-scale variability in a 54 000-year record of total air content from the South Pole ice core, *The Cryosphere*, 17, 4837–4851, <https://doi.org/10.5194/tc-17-4837-2023>, 2023.
- Etheridge, D. and Wookey, C.: Ice core drilling at a high accumulation area of Law Dome, Antarctica, 1987, in: *Ice Core Drilling, Proceedings of the Third International Workshop on Ice Core Drilling Technology*, Grenoble, France, pp. 86–96, 1988.
- Etheridge, D. M., Steele, L., Langenfelds, R. L., Francey, R. J., Barnola, J.-M., and Morgan, V.: Natural and anthropogenic changes in atmospheric CO<sub>2</sub> over the last 1000 years from air in Antarctic ice and firn, *Journal of Geophysical Research: Atmospheres*, 101, 4115–4128, <https://doi.org/10.1029/95JD03410>, 1996.
- Extier, T., Landais, A., Bréant, C., Prié, F., Bazin, L., Dreyfus, G., Roche, D. M., and Leuenberger, M.: On the use of  $\delta^{18}\text{O}_{\text{atm}}$  for ice core dating, *Quaternary Science Reviews*, 185, 244–257, <https://doi.org/https://doi.org/10.1016/j.quascirev.2018.02.008>, 2018.
- Fegyveresi, J. M., Alley, R., Spencer, M., Fitzpatrick, J., Steig, E., White, J., McConnell, J., and Taylor, K.: Late-Holocene climate evolution at the WAIS Divide site, West Antarctica: bubble number-density estimates, *Journal of Glaciology*, 57, 629–638, <https://doi.org/10.3189/002214311797409677>, 2011.

- 720 Fitzpatrick, J. J., Voigt, D. E., Fegyveresi, J. M., Stevens, N. T., Spencer, M. K., Cole-Dai, J., Alley, R. B., Jardine, G. E., Cravens, E. D., Wilen, L. A., and et al.: Physical properties of the WAIS Divide ice core, *Journal of Glaciology*, 60, 1181–1198, <https://doi.org/10.3189/2014JoG14J100>, 2014.
- Flanner, M. G. and Zender, C. S.: Linking snowpack microphysics and albedo evolution, *Journal of Geophysical Research: Atmospheres*, 111, <https://doi.org/https://doi.org/10.1029/2005JD006834>, 2006.
- 725 Freitag, J., Wilhelms, F., and Kipfstuhl, S.: Microstructure-dependent densification of polar firn derived from X-ray microtomography, *Journal of Glaciology*, 50, 243–250, <https://doi.org/10.3189/172756504781830123>, 2004.
- Frezzotti, M., Pouchet, M., Flora, O., Gandolfi, S., Gay, M., Urbini, S., Vincent, C., Becagli, S., Gragnani, R., Proposito, M., et al.: New estimations of precipitation and surface sublimation in East Antarctica from snow accumulation measurements, *Climate Dynamics*, 23, 803–813, <https://doi.org/10.1007/s00382-004-0462-5>, 2004.
- 730 Fudge, T. J., Buizert, C., Conway, H., and Waddington, E. D.: Accumulation Rates from the WAIS Divide Ice Core, <https://doi.org/110.15784/601004>, 2017.
- Fujita, S., Kawada, K., and Fujii, Y.: Glaciological Data Collected by the 37th Japanese Antarctic Research Expedition during 1996–1997, *JARE data reports*, 27, 1–46, <https://doi.org/10.15094/00004965>, 1998.
- Fujita, S., Okuyama, J., Hori, A., and Hondoh, T.: Metamorphism of stratified firn at Dome Fuji, Antarctica: A mechanism for local insolation modulation of gas transport conditions during bubble close off, *Journal of Geophysical Research: Earth Surface*, 114, <https://doi.org/https://doi.org/10.1029/2008JF001143>, 2009.
- 735 Gallet, J.-C., Domine, F., and Dumont, M.: Measuring the specific surface area of wet snow using 1310 nm reflectance, *The Cryosphere*, 8, 1139–1148, <https://doi.org/10.5194/tc-8-1139-2014>, 2014.
- Gkinis, V., Vinther, B. M., Popp, T. J., Quistgaard, T., Faber, A.-K., Holme, C. T., Jensen, C.-M., Lanzky, M., Lütt, A.-M., Mandrakis, V., et al.: A 120,000-year long climate record from a NW-Greenland deep ice core at ultra-high resolution, *Scientific data*, 8, 141, <https://doi.org/10.1038/s41597-021-00916-9>, 2021.
- 740 Gow, A., Meese, D., Alley, R., Fitzpatrick, J., Anandakrishnan, S., Woods, G., and Elder, B.: Physical and structural properties of the Greenland Ice Sheet Project 2 ice core: A review, *Journal of Geophysical Research: Oceans*, 102, 26 559–26 575, <https://doi.org/10.1029/97JC00165>, 1997.
- 745 Gow, A. J. and Meese, D.: Physical properties, crystalline textures and c-axis fabrics of the Siple Dome (Antarctica) ice core, *Journal of Glaciology*, 53, 573–584, <https://doi.org/10.3189/002214307784409252>, 2007.
- Gregory, S. A., Albert, M. R., and Baker, I.: Impact of physical properties and accumulation rate on pore close-off in layered firn, *The Cryosphere*, 8, 91–105, <https://doi.org/10.5194/tc-8-91-2014>, 2014.
- Grenfell, T. C., Warren, S. G., and Mullen, P. C.: Reflection of solar radiation by the Antarctic snow surface at ultraviolet, visible, and near-infrared wavelengths, *Journal of Geophysical Research: Atmospheres*, 99, 18 669–18 684, <https://doi.org/10.1029/94JD01484>, 1994.
- 750 Hersbach, H., Bell, B., Berrisford, P., Hirahara, S., Horányi, A., Muñoz-Sabater, J., Nicolas, J., Peubey, C., Radu, R., Schepers, D., et al.: The ERA5 global reanalysis, *Quarterly Journal of the Royal Meteorological Society*, 146, 1999–2049, <https://doi.org/10.1002/qj.3803>, 2020.
- Hoffmann, H. M., Grieman, M. M., King, A. C., Epifanio, J. A., Martin, K., Vladimirova, D., Pryer, H. V., Doyle, E., Schmidt, A., Humby, J. D., et al.: The ST22 chronology for the Skytrain Ice Rise ice core–Part 1: A stratigraphic chronology of the last 2000 years, *Climate of the Past*, 18, 1831–1847, <https://doi.org/10.5194/cp-18-1831-2022>, 2022.
- 755 Hörhold, M., Kipfstuhl, S., Wilhelms, F., Freitag, J., and Frenzel, A.: The densification of layered polar firn, *Journal of Geophysical Research: Earth Surface*, 116, <https://doi.org/10.1029/2009JF001630>, 2011.

- Hörhold, M., Laepple, T., Freitag, J., Bigler, M., Fischer, H., and Kipfstuhl, S.: On the impact of impurities on the densification of polar firn, *Earth and Planetary Science Letters*, 325, 93–99, <https://doi.org/https://doi.org/10.1016/j.epsl.2011.12.022>, 2012.
- 760 Huber, C., Beyerle, U., Leuenberger, M., Schwander, J., Kipfer, R., Spahni, R., Severinghaus, J., and Weiler, K.: Evidence for molecular size dependent gas fractionation in firn air derived from noble gases, oxygen, and nitrogen measurements, *Earth and Planetary Science Letters*, 243, 61–73, <https://doi.org/https://doi.org/10.1016/j.epsl.2005.12.036>, 2006.
- Hutterli, M. A., Schneebeli, M., Freitag, J., Kipfstuhl, J., and Röthlisberger, R.: Impact of local insolation on snow metamorphism and ice core records, *Physics of Ice Core Records II*, 68, 223–232, <http://hdl.handle.net/2115/45450>, 2009.
- 765 Ikeda-Fukazawa, T., Hondoh, T., Fukumura, T., Fukazawa, H., and Mae, S.: Variation in N<sub>2</sub>/O<sub>2</sub> ratio of occluded air in Dome Fuji antarctic ice, *Journal of Geophysical Research: Atmospheres*, 106, 17 799–17 810, <https://doi.org/10.1029/2000JD000104>, 2001.
- Ikeda-Fukazawa, T., Kawamura, K., and Hondoh, T.: Mechanism of Molecular Diffusion in Ice Crystals, *Molecular Simulation*, 30, 973–979, <https://doi.org/10.1080/08927020410001709307>, 2004.
- Ikeda-Fukazawa, T., Fukumizu, K., Kawamura, K., Aoki, S., Nakazawa, T., and Hondoh, T.: Effects of molecular diffusion on trapped gas composition in polar ice cores, *Earth and Planetary Science Letters*, 229, 183–192, <https://doi.org/https://doi.org/10.1016/j.epsl.2004.11.011>, 2005.
- 770 Inoue, R., Fujita, S., Kawamura, K., Oyabu, I., Nakazawa, F., and Motoyama, H.: Evolution of layered density and microstructure in near-surface firn around Dome Fuji, *Antarctica, EGU sphere*, 2023, 1–43, <https://doi.org/10.5194/egusphere-2023-1838>, 2023.
- Jouzel, J., Masson-Delmotte, V., Cattani, O., Dreyfus, G., Falourd, S., Hoffmann, G., Minster, B., Nouet, J., Barnola, J.-M., 775 Chappellaz, J., et al.: Orbital and millennial Antarctic climate variability over the past 800,000 years, *science*, 317, 793–796, <https://doi.org/10.1126/science.1141038>, 2007.
- Kahle, E., Buizert, C., Conway, H., Epifanio, J., Fudge, T. J., and Jones, T. R.: Temperature, accumulation rate, and layer thinning from the South Pole ice core (SPC14), <https://doi.org/10.15784/601396>, 2020.
- Kawamura, K., Parrenin, F., Lisiecki, L., Uemura, R., Vimeux, F., Severinghaus, J. P., Hutterli, M. A., Nakazawa, T., Aoki, S., 780 Jouzel, J., et al.: Northern Hemisphere forcing of climatic cycles in Antarctica over the past 360,000 years, *Nature*, 448, 912–916, <https://doi.org/10.1038/nature06015>, 2007.
- Kawamura, K., Motoyama, H., Goto-Azuma, K., Uemura, R., and Oyabu, I.: Dome Fuji Oxygen Isotope and Dust Data over the past 720 ka, <https://doi.org/https://doi.org/10.25921/zphz-qz79>, 2017.
- Kobashi, T., Ikeda-Fukazawa, T., Suwa, M., Schwander, J., Kameda, T., Lundin, J., Hori, A., Motoyama, H., Döring, M., and Leuenberger, 785 M.: Post-bubble close-off fractionation of gases in polar firn and ice cores: effects of accumulation rate on permeation through overloading pressure, *Atmospheric Chemistry and Physics*, 15, 13 895–13 914, <https://doi.org/10.5194/acp-15-13895-2015>, 2015.
- Landais, A., Chappellaz, J., Delmotte, M., Jouzel, J., Blunier, T., Bourg, C., Caillon, N., Cherrier, S., Malaizé, B., Masson-Delmotte, V., Raynaud, D., Schwander, J., and Steffensen, J. P.: A tentative reconstruction of the last interglacial and glacial inception in Greenland based on new gas measurements in the Greenland Ice Core Project (GRIP) ice core, *Journal of Geophysical Research: Atmospheres*, 108, 790 <https://doi.org/https://doi.org/10.1029/2002JD003147>, 2003.
- Landais, A., Barnola, J., Kawamura, K., Caillon, N., Delmotte, M., Van Ommen, T., Dreyfus, G., Jouzel, J., Masson-Delmotte, V., Minster, B., Freitag, J., Leuenberger, M., Schwander, J., Huber, C., Etheridge, D., and Morgan, V.: Firn-air  $\delta^{15}\text{N}$  in modern polar sites and glacial–interglacial ice: a model-data mismatch during glacial periods in Antarctica?, *Quaternary Science Reviews*, 25, 49–62, <https://doi.org/https://doi.org/10.1016/j.quascirev.2005.06.007>, 2006.

- 795 Landais, A., Dreyfus, G., Capron, E., Pol, K., Loutre, M. F., Raynaud, D., Lipenkov, V. Y., Arnaud, L., Masson-Delmotte, V., Paillard, D., Jouzel, J., and Leuenberger, M.: Towards orbital dating of the EPICA Dome C ice core using  $\delta^{15}\text{O}_2/\text{N}_2$ , *Climate of the Past*, 8, 191–203, <https://doi.org/10.5194/cp-8-191-2012>, 2012.
- Laskar, J., Robutel, P., Joutel, F., Gastineau, M., Correia, A. C. M., and Levrard, B.: A long-term numerical solution for the insolation quantities of the Earth, *AA*, 428, 261–285, <https://doi.org/10.1051/0004-6361:20041335>, 2004.
- 800 Lazzara, M. A., Keller, L. M., Markle, T., and Gallagher, J.: Fifty-year Amundsen–Scott South Pole station surface climatology, *Atmospheric Research*, 118, 240–259, <https://doi.org/https://doi.org/10.1016/j.atmosres.2012.06.027>, 2012.
- Lee, J. E., Brook, E. J., Bertler, N. A. N., Buizert, C., Baisden, T., Blunier, T., Ciobanu, V. G., Conway, H., Dahl-Jensen, D., Fudge, T. J., Hindmarsh, R., Keller, E. D., Parrenin, F., Severinghaus, J. P., Vallelonga, P., Waddington, E. D., and Winstrup, M.: An 83 000-year-old ice core from Roosevelt Island, Ross Sea, Antarctica, *Climate of the Past*, 16, 1691–1713, <https://doi.org/10.5194/cp-16-1691-2020>, 2020.
- 805 Legagneux, L., Cabanes, A., and Dominé, F.: Measurement of the specific surface area of 176 snow samples using methane adsorption at 77 K, *Journal of Geophysical Research: Atmospheres*, 107, ACH–5, <https://doi.org/10.1029/2001JD001016>, 2002.
- Legagneux, L., Lauzier, T., Domin, F., Kuhs, W. F., Heinrichs, T., and Techmer, K.: Rate of decay of specific surface area of snow during isothermal experiments and morphological changes studied by scanning electron microscopy, *Canadian Journal of Physics*, 81, 459–468, <https://doi.org/10.1139/p03-025>, 2003.
- 810 Leinss, S., Löwe, H., Proksch, M., and Kontu, A.: Modeling the evolution of the structural anisotropy of snow, *The Cryosphere*, 14, 51–75, <https://doi.org/10.5194/tc-14-51-2020>, 2020.
- Libois, Q., Picard, G., France, J. L., Arnaud, L., Dumont, M., Carmagnola, C. M., and King, M. D.: Influence of grain shape on light penetration in snow, *The Cryosphere*, 7, 1803–1818, <https://doi.org/10.5194/tc-7-1803-2013>, 2013.
- Libois, Q., Picard, G., Arnaud, L., Morin, S., and Brun, E.: Modeling the impact of snow drift on the decameter-scale variability of snow properties on the Antarctic Plateau, *Journal of Geophysical Research: Atmospheres*, 119, 11,662–11,681, <https://doi.org/https://doi.org/10.1002/2014JD022361>, 2014.
- 815 Libois, Q., Picard, G., Arnaud, L., Dumont, M., Lafaysse, M., Morin, S., and Lefebvre, E.: Summertime evolution of snow specific surface area close to the surface on the Antarctic Plateau, *The Cryosphere*, 9, 2383–2398, <https://doi.org/10.5194/tc-9-2383-2015>, 2015.
- Lipenkov, V., Raynaud, D., Loutre, M., and Duval, P.: On the potential of coupling air content and  $\text{O}_2/\text{N}_2$  from trapped air for establishing an ice core chronology tuned on local insolation, *Quaternary Science Reviews*, 30, 3280–3289, <https://doi.org/https://doi.org/10.1016/j.quascirev.2011.07.013>, 2011.
- 820 Lüthi, D., Bereiter, B., Stauffer, B., Winkler, R., Schwander, J., Kindler, P., Leuenberger, M., Kipfstuhl, S., Capron, E., Landais, A., Fischer, H., and Stocker, T. F.:  $\text{CO}_2$  and  $\text{O}_2/\text{N}_2$  variations in and just below the bubble–clathrate transformation zone of Antarctic ice cores, *Earth and Planetary Science Letters*, 297, 226–233, <https://doi.org/https://doi.org/10.1016/j.epsl.2010.06.023>, 2010.
- 825 Martin, K. C., Buizert, C., Edwards, J. S., Kalk, M. L., Riddell-Young, B., Brook, E. J., Beaudette, R., Severinghaus, J. P., and Sowers, T. A.: Bipolar impact and phasing of Heinrich-type climate variability, *Nature*, pp. 1–5, <https://doi.org/10.1038/s41586-023-05875-2>, 2023.
- Martinerie, P., Lipenkov, V. Y., Raynaud, D., Chapellaz, J., Barkov, N. I., and Lorius, C.: Air content paleo record in the Vostok ice core (Antarctica): A mixed record of climatic and glaciological parameters, *Journal of Geophysical Research: Atmospheres*, 99, 10 565–10 576, <https://doi.org/https://doi.org/10.1029/93JD03223>, 1994.
- 830 Martinerie, P., Nourtier-Mazaure, E., Barnola, J.-M., Sturges, W. T., Worton, D. R., Atlas, E., Gohar, L. K., Shine, K. P., and Brasseur, G. P.: Long-lived halocarbon trends and budgets from atmospheric chemistry modelling constrained with measurements in polar firn, *Atmospheric Chemistry and Physics*, 9, 3911–3934, <https://doi.org/10.5194/acp-9-3911-2009>, 2009.



- Massam, A.: Modelling the age-depth and temperature profiles of deep ice cores from the Antarctic Peninsula and the Weddell Sea region, Phd thesis, University of Durham, available at <https://nora.nerc.ac.uk/id/eprint/520454/>, 2018.
- 835 Matsuoka, K., Skoglund, A., and Roth, G.: Quantarctica, <https://doi.org/10.21334/npolar.2018.8516e961>, 2018.
- Mitchell, L. E., Buizert, C., Brook, E. J., Breton, D. J., Fegyveresi, J., Baggenstos, D., Orsi, A., Severinghaus, J., Alley, R. B., Albert, M., Rhodes, R. H., McConnell, J. R., Sigl, M., Maselli, O., Gregory, S., and Ahn, J.: Observing and modeling the influence of layering on bubble trapping in polar firn, *Journal of Geophysical Research: Atmospheres*, 120, 2558–2574, <https://doi.org/https://doi.org/10.1002/2014JD022766>, 2015.
- 840 Moon, T. A., Fisher, M., Stafford, T., and Thurber, A.: QGreenland (v3), 2023.
- Morgan, V., Wookey, C., Li, J., van Ommen, T., Skinner, W., and Fitzpatrick, : Site information and initial results from deep ice drilling on Law Dome, Antarctica, *Journal of Glaciology*, 43, 3–10, <https://doi.org/10.3189/S0022143000002768>, 1997.
- Mulvaney, R., Alemany, O., and Possenti, P.: The Berkner Island (Antarctica) ice-core drilling project, *Annals of Glaciology*, 47, 115–124, <https://doi.org/10.3189/172756407786857758>, 2007.
- 845 Mulvaney, R., Abram, N. J., Hindmarsh, R. C., Arrowsmith, C., Fleet, L., Triest, J., Sime, L. C., Alemany, O., and Foord, S.: Recent Antarctic Peninsula warming relative to Holocene climate and ice-shelf history, *Nature*, 489, 141–144, <https://doi.org/10.1038/nature11391>, 2012.
- Mulvaney, R., Triest, J., and Alemany, O.: The James Ross Island and the Fletcher Promontory ice-core drilling projects, *Annals of Glaciology*, 55, 179–188, <https://doi.org/10.3189/2014AoG68A044>, 2014.
- Mulvaney, R., Rix, J., Polfrey, S., Grieman, M., Martìn, C., Nehrbass-Ahles, C., Rowell, I., Tuckwell, R., and Wolff, E.: Ice drilling on Skytrain Ice Rise and Sherman Island, Antarctica, *Annals of Glaciology*, 62, 311–323, <https://doi.org/10.1017/aog.2021.7>, 2021.
- 850 Mulvaney, R., Wolff, E. W., Grieman, M. M., Hoffmann, H. H., Humby, J. D., Nehrbass-Ahles, C., Rhodes, R. H., Rowell, I. F., Parrenin, F., Schmidely, L., et al.: The ST22 chronology for the Skytrain Ice Rise ice core–Part 2: An age model to the last interglacial and disturbed deep stratigraphy, *Climate of the Past*, 19, 851–864, <https://doi.org/10.5194/cp-19-851-2023>, 2023.
- NEEM Community Members: Eemian interglacial reconstructed from a Greenland folded ice core, *Nature*, 493, 489–494, <https://doi.org/10.1038/nature11789>, 2013.
- 855 Neff, P. D.: A review of the brittle ice zone in polar ice cores, *Annals of Glaciology*, 55, 72–82, <https://doi.org/10.3189/2014AoG68A023>, 2014.
- NGRIP project members: High-resolution record of Northern Hemisphere climate extending into the last interglacial period, *Nature*, 431, 147–151, <https://doi.org/10.1038/nature02805>, 2004.
- 860 Oyabu, I., Kawamura, K., Uchida, T., Fujita, S., Kitamura, K., Hirabayashi, M., Aoki, S., Morimoto, S., Nakazawa, T., Severinghaus, J. P., and Morgan, J. D.: Fractionation of O<sub>2</sub>/N<sub>2</sub> and Ar/N<sub>2</sub> in the Antarctic ice sheet during bubble formation and bubble-clathrate hydrate transition from precise gas measurements of the Dome Fuji ice core, *The Cryosphere*, 15, 5529–5555, <https://doi.org/10.5194/tc-15-5529-2021>, 2021.
- Oyabu, I., Kawamura, K., Buizert, C., Parrenin, F., Orsi, A., Kitamura, K., Aoki, S., and Nakazawa, T.: The Dome Fuji ice core DF2021 chronology (0–207 kyr BP), *Quaternary Science Reviews*, 294, 107 754, <https://doi.org/10.1016/j.quascirev.2022.107754>, 2022.
- 865 Parrenin, F., Barnola, J.-M., Beer, J., Blunier, T., Castellano, E., Chappellaz, J., Dreyfus, G., Fischer, H., Fujita, S., Jouzel, J., et al.: The EDC3 chronology for the EPICA Dome C ice core, *Climate of the Past*, 3, 485–497, <https://doi.org/10.5194/cp-3-485-2007>, 2007.
- Parrenin, F., Petit, J.-R., Masson-Delmotte, V., Wolff, E., Basile-Doelsch, I., Jouzel, J., Lipenkov, V., Rasmussen, S., Schwander, J., Severi, M., et al.: Volcanic synchronisation between the EPICA Dome C and Vostok ice cores (Antarctica) 0–145 kyr BP, *Climate of the Past*, 8, 1031–1045, <https://doi.org/10.5194/cp-8-1031-2012>, 2012.
- 870

- Petit, J.-R., Jouzel, J., Raynaud, D., Barkov, N. I., Barnola, J.-M., Basile, I., Bender, M., Chappellaz, J., Davis, M., Delaygue, G., et al.: Climate and atmospheric history of the past 420,000 years from the Vostok ice core, Antarctica, *Nature*, 399, 429–436, <https://doi.org/10.1038/20859>, 1999.
- Petrenko, V. V., Severinghaus, J. P., Brook, E. J., Reeh, N., and Schaefer, H.: Gas records from the West Greenland ice margin covering the Last Glacial Termination: a horizontal ice core, *Quaternary Science Reviews*, 25, 865–875, <https://doi.org/https://doi.org/10.1016/j.quascirev.2005.09.005>, 2006.
- Picard, G., Domine, F., Krinner, G., Arnaud, L., and Lefebvre, E.: Inhibition of the positive snow-albedo feedback by precipitation in interior Antarctica, *Nature Climate Change*, 2, 795–798, <https://doi.org/10.1038/nclimate1590>, 2012.
- Rasmussen, S. O., Abbott, P. M., Blunier, T., Bourne, A., Brook, E., Buchardt, S. L., Buizert, C., Chappellaz, J., Clausen, H., Cook, E., et al.: A first chronology for the North Greenland Eemian Ice Drilling (NEEM) ice core, *Climate of the Past*, 9, 2713–2730, <https://doi.org/10.5194/cp-9-2713-2013>, 2013.
- Raynaud, D., Lipenkov, V., Lemieux-Dudon, B., Duval, P., Loutre, M.-F., and Lhomme, N.: The local insolation signature of air content in Antarctic ice. A new step toward an absolute dating of ice records, *Earth and Planetary Science Letters*, 261, 337–349, <https://doi.org/https://doi.org/10.1016/j.epsl.2007.06.025>, 2007.
- Rubino, M., Etheridge, D. M., Thornton, D. P., Howden, R., Allison, C. E., Francey, R. J., Langenfelds, R. L., Steele, L. P., Trudinger, C. M., Spencer, D. A., Curran, M. A. J., van Ommen, T. D., and Smith, A. M.: Revised records of atmospheric trace gases CO<sub>2</sub>, CH<sub>4</sub>, N<sub>2</sub>O, and δ<sup>13</sup>C-CO<sub>2</sub> over the last 2000 years from Law Dome, Antarctica, *Earth System Science Data*, 11, 473–492, <https://doi.org/10.5194/essd-11-473-2019>, 2019.
- Schaefer, H., Lourantou, A., Chappellaz, J., Lüthi, D., Bereiter, B., and Barnola, J.-M.: On the suitability of partially clathrated ice for analysis of concentration and δ<sup>13</sup>C of palaeo-atmospheric CO<sub>2</sub>, *Earth and planetary science letters*, 307, 334–340, <https://doi.org/10.1016/j.epsl.2011.05.007>, 2011.
- Schwander, J., Sowers, T., Barnola, J.-M., Blunier, T., Fuchs, A., and Malaizé, B.: Age scale of the air in the summit ice: Implication for glacial-interglacial temperature change, *Journal of Geophysical Research: Atmospheres*, 102, 19483–19493, <https://doi.org/https://doi.org/10.1029/97JD01309>, 1997.
- Severinghaus, J.: Nitrogen and Oxygen Gas Isotopes in the Siple Dome and Byrd Ice Cores, Antarctica [Dataset], <https://doi.org/10.7265/N55X26V0>, 2009.
- Severinghaus, J.: Low-res d15N and d18O of O2 in the WAIS Divide 06A Deep Core [Dataset], <https://doi.org/10.7265/N5S46PWD>, 2015.
- Severinghaus, J.: South Pole (SPICECORE) 15N, 18O, O2/N2 and Ar/N2 [Dataset], <https://doi.org/10.15784/601152>, 2019.
- Severinghaus, J. P. and Battle, M. O.: Fractionation of gases in polar ice during bubble close-off: New constraints from firm air Ne, Kr and Xe observations, *Earth and Planetary Science Letters*, 244, 474–500, <https://doi.org/https://doi.org/10.1016/j.epsl.2006.01.032>, 2006.
- Severinghaus, J. P., Grachev, A., and Battle, M.: Thermal fractionation of air in polar firm by seasonal temperature gradients, *Geochemistry, Geophysics, Geosystems*, 2, <https://doi.org/10.1029/2000GC000146>, 2001.
- Shackleton, S. A.: Tracking Past Changes in Ocean Heat Content with Atmospheric Noble Gases in Ice Cores, Doctoral dissertation, University of California, San Diego, <http://dissertations.umi.com/ucsd:18809>, 2019.
- Smith, M. E.: The Pleistocene O<sub>2</sub> record in two ice cores, 1998.
- Sowers, T., Bender, M., and Raynaud, D.: Elemental and isotopic composition of occluded O<sub>2</sub> and N<sub>2</sub> in polar ice, *Journal of Geophysical Research: Atmospheres*, 94, 5137–5150, <https://doi.org/https://doi.org/10.1029/JD094iD04p05137>, 1989.

- Stenni, B., Proposito, M., Gragnani, R., Flora, O., Jouzel, J., Falourd, S., and Frezzotti, M.: Eight centuries of volcanic signal and climate change at Talos Dome (East Antarctica), *Journal of Geophysical Research: Atmospheres*, 107, ACL-3, <https://doi.org/10.1029/2000JD000317>, 2002.
- 910 Stenni, B., Masson-Delmotte, V., Selmo, E., Oerter, H., Meyer, H., Röthlisberger, R., Jouzel, J., Cattani, O., Falourd, S., Fischer, H., Hoffmann, G., Iacumin, P., Johnsen, S., Minster, B., and Udisti, R.: The deuterium excess records of EPICA Dome C and Dronning Maud Land ice cores (East Antarctica), *Quaternary Science Reviews*, 29, 146–159, <https://doi.org/https://doi.org/10.1016/j.quascirev.2009.10.009>, climate of the Last Million Years: New Insights from EPICA and Other Records, 2010.
- 915 Suwa, M. and Bender, M. L.: Chronology of the Vostok ice core constrained by O<sub>2</sub>/N<sub>2</sub> ratios of occluded air, and its implication for the Vostok climate records, *Quaternary Science Reviews*, 27, 1093–1106, <https://doi.org/https://doi.org/10.1016/j.quascirev.2008.02.017>, 2008a.
- Suwa, M. and Bender, M. L.: O<sub>2</sub>/N<sub>2</sub> ratios of occluded air in the GISP2 ice core, *Journal of Geophysical Research: Atmospheres*, 113, <https://doi.org/https://doi.org/10.1029/2007JD009589>, 2008b.
- Uchida, T., Duval, P., Lipenkov, V. Y., Hondoh, T., Mae, S., and Shoji, H.: Brittle zone and air-hydrate formation in polar ice sheets, *Memoirs of National Institute of Polar Research. Special issue*, 49, 298–305, [http://purl.org/coar/resource\\_type/c\\_6501](http://purl.org/coar/resource_type/c_6501), 1994.
- Ueltzhöffer, K. J., Bendel, V., Freitag, J., Kipfstuhl, S., Wagenbach, D., Faria, S. H., and Garbe, C. S.: Distribution of air bubbles in the EDML and EDC (Antarctica) ice cores, using a new method of automatic image analysis, *Journal of Glaciology*, 56, 339–348, <https://doi.org/10.3189/002214310791968511>, 2010.
- 925 Uemura, R., Motoyama, H., Masson-Delmotte, V., Jouzel, J., Kawamura, K., Goto-Azuma, K., Fujita, S., Kuramoto, T., Hirabayashi, M., Miyake, T., et al.: Asynchrony between Antarctic temperature and CO<sub>2</sub> associated with obliquity over the past 720,000 years, *Nature communications*, 9, 961, <https://doi.org/10.1038/s41467-018-03328-3>, 2018.
- Vionnet, V., Brun, E., Morin, S., Boone, A., Faroux, S., Le Moigne, P., Martin, E., and Willemet, J.-M.: The detailed snowpack scheme Crocus and its implementation in SURFEX v7.2, *Geoscientific Model Development*, 5, 773–791, <https://doi.org/10.5194/gmd-5-773-2012>, 2012.
- Warming, E., Svensson, A., Vallelonga, P., and Bigler, M.: A technique for continuous detection of drill liquid in ice cores, *Journal of glaciology*, 59, 503–506, <https://doi.org/10.3189/2013JoG12J124>, 2013.
- 930 Warren, S. G., Brandt, R. E., and Grenfell, T. C.: Visible and near-ultraviolet absorption spectrum of ice from transmission of solar radiation into snow, *Appl. Opt.*, 45, 5320–5334, <https://doi.org/10.1364/AO.45.005320>, 2006.
- White, J., Bradley, E., Garland, J., Jones, T. R., Morris, V., Price, M., and Vaughn, B.: Stable Isotopes of Ice in the Transition and Glacial Sections of the WAIS Divide Deep Ice Core, <https://doi.org/10.15784/601274>, 2019.
- 935 Winstrup, M., Vallelonga, P., Kjær, H. A., Fudge, T. J., Lee, J. E., Riis, M. H., Edwards, R., Bertler, N. A. N., Blunier, T., Brook, E. J., Buizert, C., Ciobanu, G., Conway, H., Dahl-Jensen, D., Ellis, A., Emanuelsson, B. D., Hindmarsh, R. C. A., Keller, E. D., Kurbatov, A. V., Mayewski, P. A., Neff, P. D., Pyne, R. L., Simonsen, M. F., Svensson, A., Tuohy, A., Waddington, E. D., and Wheatley, S.: A 2700-year annual timescale and accumulation history for an ice core from Roosevelt Island, West Antarctica, *Climate of the Past*, 15, 751–779, <https://doi.org/10.5194/cp-15-751-2019>, 2019.
- 940 Witrant, E., Martinerie, P., Hogan, C., Laube, J., Kawamura, K., Capron, E., Montzka, S., Dlugokencky, E., Etheridge, D., Blunier, T., et al.: A new multi-gas constrained model of trace gas non-homogeneous transport in firn: evaluation and behaviour at eleven polar sites, *Atmospheric Chemistry and Physics*, 12, 11 465–11 483, <https://doi.org/10.5194/acp-12-11465-2012>, 2012.